



Geochronological and geochemical evidences for extension-related Neoproterozoic granitoids in the southern São Francisco Craton, Brazil

J.A. Moreno^{a,*}, M.R. Baldim^a, J. Semprich^a, E.P. Oliveira^a, S.K. Verma^b, W. Teixeira^c

^a Department of Geology and Natural Resources, Institute of Geosciences, PO Box 6152, University of Campinas – UNICAMP, 13083-970 Campinas, SP, Brazil

^b División de Geociencias Aplicadas, Instituto Potosino de Investigación Científica y Tecnológica (IPICYT), Camino a la Presa San José 2055, San Luis Potosí 78216, Mexico

^c Instituto de Geociências, Universidade de São Paulo, Rua do Lago, 562, 05508-080 São Paulo, SP, Brazil

ARTICLE INFO

Article history:

Received 22 December 2016

Revised 22 March 2017

Accepted 2 April 2017

Available online 6 April 2017

Keywords:

A-type magmatism

Extensional setting

Continental crust

Juvenile source

São Francisco Craton

ABSTRACT

New LA-SF-ICP-MS U-Pb zircon dating of high-K granitoids from the Campo Belo metamorphic complex, southern São Francisco Craton (Brazil), reveals a long period (ca. 100 My) of Neoproterozoic granitic magmatism that post-date the TTG magmatism. The oldest studied pluton is a highly porphyritic biotite orthogneiss emplaced at 2748 ± 5 Ma, followed by a hornblende-biotite orthogneiss (2727 ± 7 Ma). Both granitic bodies were affected by a deformation event prior to the emplacement of the Rio do Amparo, Bom Sucesso and Lavras granitoid plutons at 2716 ± 6 Ma, 2696 ± 6 Ma and 2646 ± 5 Ma, respectively. The Neoproterozoic granitic magmatism ended with the intrusion of peraluminous leucogranitic dikes at 2631 ± 4 Ma.

The 2.73–2.65 Ga Campo Belo granitoids share chemical features of A-type granites, such as high apatite- and zircon-saturation temperatures (mostly > 800 °C), relatively high Fe-number, high total alkalis and characteristic enrichment in LREE and HFSE although most samples of the Rio do Amparo granite have lower HFSE and LREE content than typical A-type granites but very high Th. The high Th content of the Rio do Amparo and Bom Sucesso granites may suggest involvement of Th-orthosilicate in their sources. The trace element composition permits to classify the Campo Belo granitoids as A₂-type granites, suggesting derivation from partial melting of TTG-crustal sources likely in an extensional setting.

Significant reworking of Mesoproterozoic crust is suggested by mostly negative ϵ_{Nd_i} values (Rio do Amparo: -2.0 and $+3.1$; Bom Sucesso: -3.6 , -3.1 and $+0.9$; Lavras: -2.5 and -0.2) and old Nd model ages (T_{DM} close to 3.1 Ga), although with probable involvement of juvenile material (T_{DM} of 2.7–2.9 Ga). This contrasts with Neoproterozoic granites of the northern São Francisco and Congo cratons characterized by negligible juvenile imprint.

The 2.75–2.63 Ga Campo Belo granitoids witness the thermal stabilization of the Archean lithosphere through a major episode of high-K granitoid magmatism between 2760 and 2600 Ma, which affected the whole São Francisco Craton and the northern Congo Craton.

© 2017 Elsevier B.V. All rights reserved.

1. Introduction

Granites and related rocks constitute the largest component of the upper continental crust, and as such, their origin is one of the most important topics in igneous petrology (Kemp and Hawkesworth, 2003; Castro, 2014; and references therein). However, despite the abundance and relatively simple mineralogy of granites (predominantly quartz, alkali feldspar and plagioclase), their petrogenesis is controversial. This is due to the fact that several factors can control the generation of granitic magmas such as different tectonic environments with contrasting mantle and

crustal sources and diverse conditions of magma formation and emplacement. Consequently, the study of granites contributes to the understanding of crustal formation, differentiation and recycling.

Most of the continental crust was formed in the Archean era, chiefly in the late Archean, although only $<10\%$ of the crust of that age is still preserved (Hawkesworth et al., 2010, 2013).

Archean cratons can be generally divided into three different lithologic units: (1) the gneissic basement composed of deformed and migmatitic meta-igneous rocks that mainly consist of low-K granitoids of the tonalite-trondhjemite-granodiorite (TTG) series; (2) the greenstone belts that comprise meta-sedimentary and meta-volcanic rocks metamorphosed from greenschist to amphibolite facies; and (3) late, medium- to high-K granitoids. Although

* Corresponding author.

E-mail addresses: jmoreno_2@ugr.es, jumoreno1983@gmail.com (J.A. Moreno).

the TTG suite is volumetrically dominant, the high-K granitoids can represent up to 20% of the exposed Archean rocks (Condie, 1993; Sylvester, 1994). Since they are relatively abundant rocks and their origin and emplacement mark the thermal stabilization of Archean lithosphere (Kusky and Polat, 1999; Laurent et al., 2014a; Tchameni et al., 2000; Romano et al., 2013), the number of works that have investigated Archean high-K granitoids has increased in the last decade (e.g., Drüppel et al., 2009; Jayananda et al., 2006; Laurent et al., 2014a; Moyen et al., 2003; Romano et al., 2013; Zhou et al., 2015). The Archean high-K magmatism is represented by different types of granitoids (e.g. sanukitoids, biotite granites, peralkaline granites, syenites, etc.; see Moyen et al., 2003 and Laurent et al., 2014a for details) of mainly crustal origin, although mantle sources and interaction between crustal and mantle end-members have also been suggested as petrogenetic processes to account for the origin of these rocks in subduction-related, collision, post-collision and intra-plate settings (Champion and Sheraton, 1997; Day and Weiblen, 1986; Frost et al., 1998; Jayananda et al., 2000; Laurent et al., 2014b; Mikkola et al., 2011; Smithies and Champion, 1999, 2000; Semprich et al., 2015; Stern et al., 1989). Furthermore, those petrogenetic processes that generated Archean granitoids are especially difficult to unravel because of our limited knowledge of plate dynamics as well as crustal and mantle compositions and P-T conditions at that time. Therefore, studies that lead to a better understanding of the petrogenesis and tectonic environments of Archean high-K granitoids can improve our knowledge of crust formation in Earth's history.

Late Archean granitoids are conspicuous in the Archean core of the southern portion of the São Francisco Craton in Brazil (Fig. 1)

(Campos et al., 2003; Lana et al., 2013; Romano et al., 2013; Teixeira et al., 1996, 1998), which represents one of the largest and oldest areas of stable continental crust in South America. It is therefore a suitable place to study the nature and origin of the ancient granitic magmatism that have been the focus of previous investigations by means of geochronology and geochemistry (e.g., Campos and Carneiro, 2008; Farina et al., 2015a; Romano et al., 2013).

The Campo Belo metamorphic complex (CBMC), located in the southern São Francisco Craton, is mainly composed of migmatitic gneisses, granulites and granitoids, accreted and migmatized in the 3100–2840 Ma time interval (Teixeira et al., 1996). However large portions of the CBMC have not been thoroughly studied yet. In fact, very few data of high-K granitoids from this complex have been published (Campos and Carneiro, 2008; Trouw et al., 2008; Quéméneur, 1996), so that this study fills this gap of knowledge in the region and constitutes a first step for further petrogenetic investigations. The present study provides new LA-SF-ICP-MS U-Pb zircon dating as well as major and trace element whole-rock and Nd isotope data of the main high-K granitoid rocks from the CBMC in order to establish the sequence of emplacement and characterize their chemical composition. These data will be used to infer plausible sources and discuss their tectonic implications as well as clarifying possible genetic relations between the different granitoids.

2. Geological setting

The São Francisco Craton (SFC), located in the eastern portion of South America (Fig. 1A), is the best-exposed and most accessible

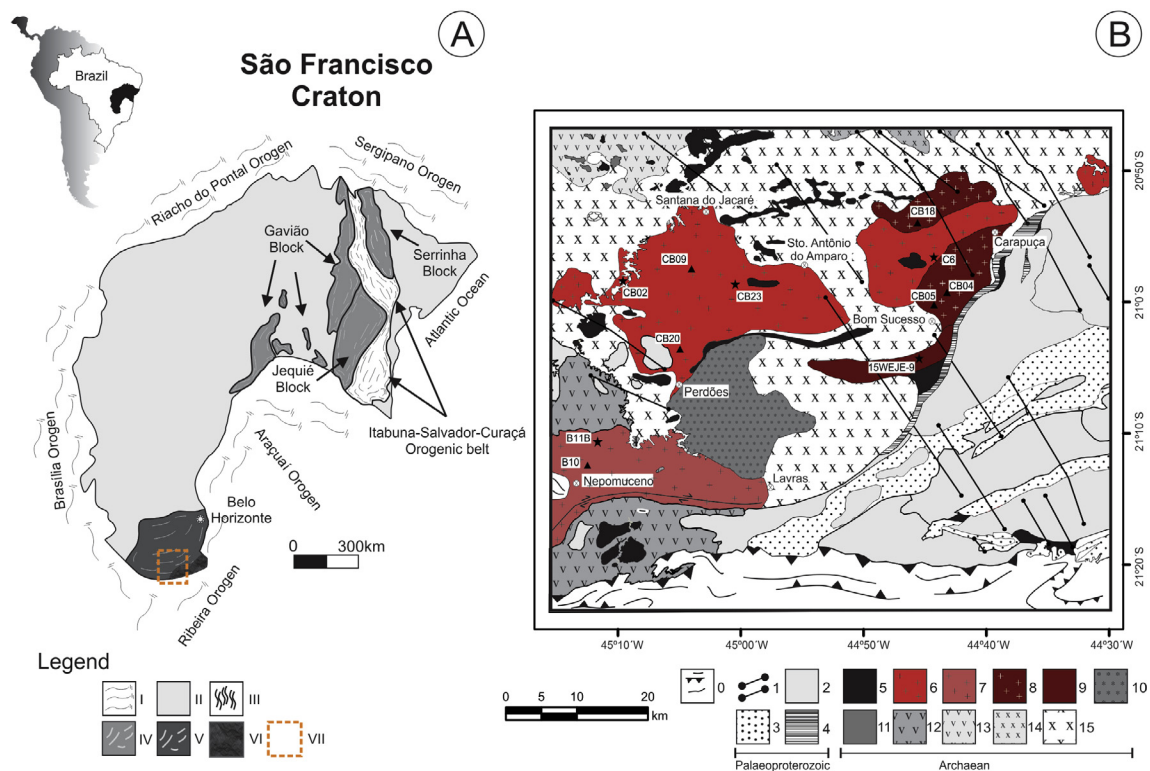


Fig. 1. Tectonic sketch of the São Francisco Craton and geological map of the studied area. (A) São Francisco Craton and its Archean-Paleoproterozoic blocks with location of the studied area. Legend: (I) Neoproterozoic orogenic belts, (II) Proterozoic and Phanerozoic covers <1.8 Ga, (III) Paleoproterozoic high-grade Itabuna-Salvador-Curaçá orogen, (IV) and (V) Archean-Paleoproterozoic basement, (VI) Paleoproterozoic mineiro belt, (VII) the studied area. (B) Simplified geological map of the Campo Belo region. Neoproterozoic belt: (0) Andrélandia-Carandaí sequences (1). Paleoproterozoic units: (1) Mafic dike swarms, (2) Diorite-granitoid crust, (3) Supracrustal sequences, (4) Minas supergroup. Archean units: (5) Ribeirão dos Motas meta-mafic-ultramafic unit, (6) Rio do Amparo pluton, (7) Lavras pluton, (8) Bom Sucesso pluton, (9) Porphyritic biotite orthogneiss, (10) Ribeirão Vermelho charnockite, (11) Sillimanite-quartzite, (12) Campos Gerais gneiss, (13) Candeias gneiss, (14) Claudio gneiss, (15) Fernão Dias gneiss. Sampling: black stars (U-Pb analysis), black triangles (Sm-Nd analysis) and black circles (U-Pb and Sm-Nd analysis). Adapted from CPRM (Brazilian Geological Survey).

segment of Precambrian basement in Brazil. Archean and Paleoproterozoic terranes of the SFC crop out in two geographically distinct areas, the first and larger one to the north and northeast of Bahia state and, the second to the south in state of Minas Gerais (Fig. 1A). The northern area is composed of different blocks, namely the Gavião, Jequié, Serrinha and Itabuna-Salvador-Curaça blocks, with intervening Paleoproterozoic belts (Barbosa and Sabaté, 2004; Teixeira and Figueiredo, 1991; Teixeira et al., 1996, 2000) whilst surrounded by the Neoproterozoic orogens of Western Gondwana.

The southern portion of the São Francisco Craton (SSFC; Fig. 1A) was formed during multiple stages of TTG and high-K granitoid magmatism in and around poly-deformed greenstone belt sequences between 3200 Ma and 2600 Ma (e.g., Carneiro, 1992; Noce, 1995; Teixeira et al., 1996; Machado et al., 1996; Lana et al., 2013). According to recent studies at the Quadrilátero Ferrífero area (Farina et al., 2015a, 2015b; Lana et al., 2013; Romano et al., 2013), the ancient nucleus of the SSFC was formed by four main orogenic events. The first, called the Santa Barbara event, is related to the generation of Paleoproterozoic TTG crust (ca. 3212–3210 Ma), as previously envisaged from inherited U-Pb SHRIMP ages in the Campo Belo migmatite (Teixeira et al., 1996, 1998). During the second event, termed the Rio das Velhas I, a Mesoarchean core was formed, represented by TTG suites and mafic-ultramafic rocks (greenstone belt-like) between 2930 and 2900 Ma. In the following event, called the Rio das Velhas II, medium-K granitoids were formed at 2800–2760 Ma, which are associated to greenstone belt sequences i.e., Rio das Velhas Supergroup (Moreira et al., 2016). Finally, the Mamona event corresponds to the cratonization and consolidation of the granitic crust between 2760 and 2680 Ma via generation and emplacement of high-K granitoids. Subsequent Paleoproterozoic reworking of the Archean crust has been pointed out by Carvalho et al. (2016, 2017) based on the ca. 2.05 Ga migmatization event recorded in the Kinawa migmatite, probably related to the collision event of the Mineiro Belt and Mantiqueira Complex with the Archean core of the SFC.

Teixeira et al. (1996, 1998) highlighted three major metamorphic complexes in this part of the craton, which are the Campo Belo, Belo Horizonte and Bonfim Complexes.

2.1. The Campo Belo metamorphic complex: field relations and rock descriptions

The Campo Belo metamorphic complex (CBMC), mostly composed of Archean rocks, is located to the west-southwest of the other two complexes and is covered by Neoproterozoic sedimentary rocks of the Bambuí Group (Fig. 1). The complex was mainly affected by amphibolite facies metamorphism although granulitic rocks have been described in some areas (Carneiro et al., 1997; Québécois, 1996; Engler et al., 2002).

The CBMC consists of migmatitic gneisses of TTG affinity (Fernão Dias, Candeias, Itapeperica and Cláudio gneisses), meta-mafic-ultramafic rocks of the Ribeirão dos Motas layered suite and the Carmópolis de Minas intrusive suite (see Goulart et al., 2013), as well as intrusive granitic bodies and relicts of supracrustal sequences (amphibolites, quartzites and schists, BIFs, metaultramafic rocks) that have been correlated with the Rio das Velhas Supergroup (Oliveira and Carneiro, 2001). However, Teixeira et al. (2017) have reported Paleoproterozoic ages for the Itapeperica graphite-rich supracrustal succession, which suggest that they cannot belong to the Rio das Velhas Supergroup. All these rocks are crosscut by meta-mafic (gabbroic to noritic) dikes, which fill major NW-SE and N-S fractures (Pinese et al., 1995; Pinese, 1997; Cederberg et al., 2016).

The oldest and most widespread unit of the CBMC is the Fernão Dias orthogneiss, which is mainly tonalitic to granodioritic in

composition and presents granoblastic to lepidoblastic textures with variable proportions of plagioclase, quartz, K-feldspar, biotite, amphibole and pyroxenes (Carneiro et al., 2007). A neosome of this migmatitic gneiss was dated by Teixeira et al. (1998), obtaining a zircon age of ca. 2.84 Ga, which was interpreted as the age of the migmatitic event. They also described inherited zircons of 3.2 and 3.05 Ga.

The Fernão Dias orthogneiss is intruded by three granitic plutons named the Rio do Amparo, Bom Sucesso and Lavras granitoids (Fig. 1B), whose study is the main objective of this work.

The Rio do Amparo pluton consists mostly of medium-grained isotropic leuco to mesocratic biotite monzogranites to syenogranites exposed over a huge area of about 280 km² between Santana do Jacaré, Perdões and Santo Antonio do Amparo (Fig. 1B). The main facies (Fig. 2B) is made of medium-grained equigranular monzogranite to syenogranite with a major mineral assemblage of subhedral alkali feldspar (30–40 vol%) and plagioclase (20–30 vol%), anhedral quartz (30–35 vol%), euhedral biotite (up to ~8 vol%) and scarce muscovite (<1 vol%) that appears included in or intergrown with biotite. The accessory assemblage is made of Fe-Ti oxides, allanite, zircon and apatite. This pluton is crosscut by meta-mafic dikes of the Timboré and Lençóis systems (Carneiro et al., 2007). It also contains mega-enclaves of ultramafic rocks that probably belong to the Ribeirão dos Motas mafic-ultramafic layered suite (Carneiro et al., 2007). Interestingly, in the middle part of the body it hosts mega-enclaves of strongly deformed amphibole-biotite granitic augen-gneiss (Fig. 2C) of meter-scale (tens of meters) with a subvertical foliation trending E-W, which seem to be lineated parallel to the foliation. Three outcrops of this orthogneiss that mainly consists of alkali feldspar, plagioclase, quartz, biotite and hornblende, have been found and sampled in this work, however, no contacts with the Rio do Amparo granite could be observed. In these samples, foliation is marked by dark narrow bands of green hornblende, biotite, titanite and less apatite. Felsic bands are composed of quartz, microcline, plagioclase, and rare perthitic feldspar, although sometimes they are made up of pure plagioclase or pure microcline. Granites from São Pedro das Carapuças pluton, located 15 km to the northeast of Carapuça city, have been traditionally ascribed to the Rio do Amparo granite and present TIMS zircon ages of ~2587 Ma (Campos, 2004).

The Bom Sucesso pluton crops out to the northeast of Bom Sucesso city with an exposure of ca. 100 km² (Fig. 1B). According to Québécois (1996), the Bom Sucesso granite consists of two facies: a gray-bluish homogeneous, medium-grained biotite syenogranite (Bom Sucesso I) that crops out in the core of the body; and a porphyritic gray biotite monzogranite (Bom Sucesso II) that appears in the eastern part of the body. Unfortunately, it was not possible to find any other field relation between the two facies. Bom Sucesso I facies consists of medium-grained, rarely fine-grained, equigranular to inequigranular monzogranites to syenogranites, which are composed of alkali feldspar (30–45 vol%), mostly microcline and subordinate perthite, quartz (30–40 vol%), plagioclase (15–25 vol%) and biotite (4–10 vol%). The accessory assemblage consists of titanite, allanite, magmatic epidote included in biotite and plagioclase, zircon, apatite and Fe-Ti oxides. Plagioclase is commonly altered to sericite. Samples with the highest colour index contain rare centimeter-scale biotite clots (Fig. 2E). Bom Sucesso II facies consists of porphyritic monzogranites with coarse-grained alkali feldspar and plagioclase phenocrysts (5 vol%) set in a medium-grained matrix of plagioclase (30–35 vol%), alkali feldspar (25–30 vol%), quartz (25–30 vol%) and biotite (~5 vol%). Small euhedral to subhedral plagioclase and quartz crystals can be found as inclusions in alkali feldspar. The accessory minerals are epidote, titanite, zircon, apatite and Fe-Ti oxides. A Rb-Sr age of 2748 Ma ± 60 Ma was obtained for

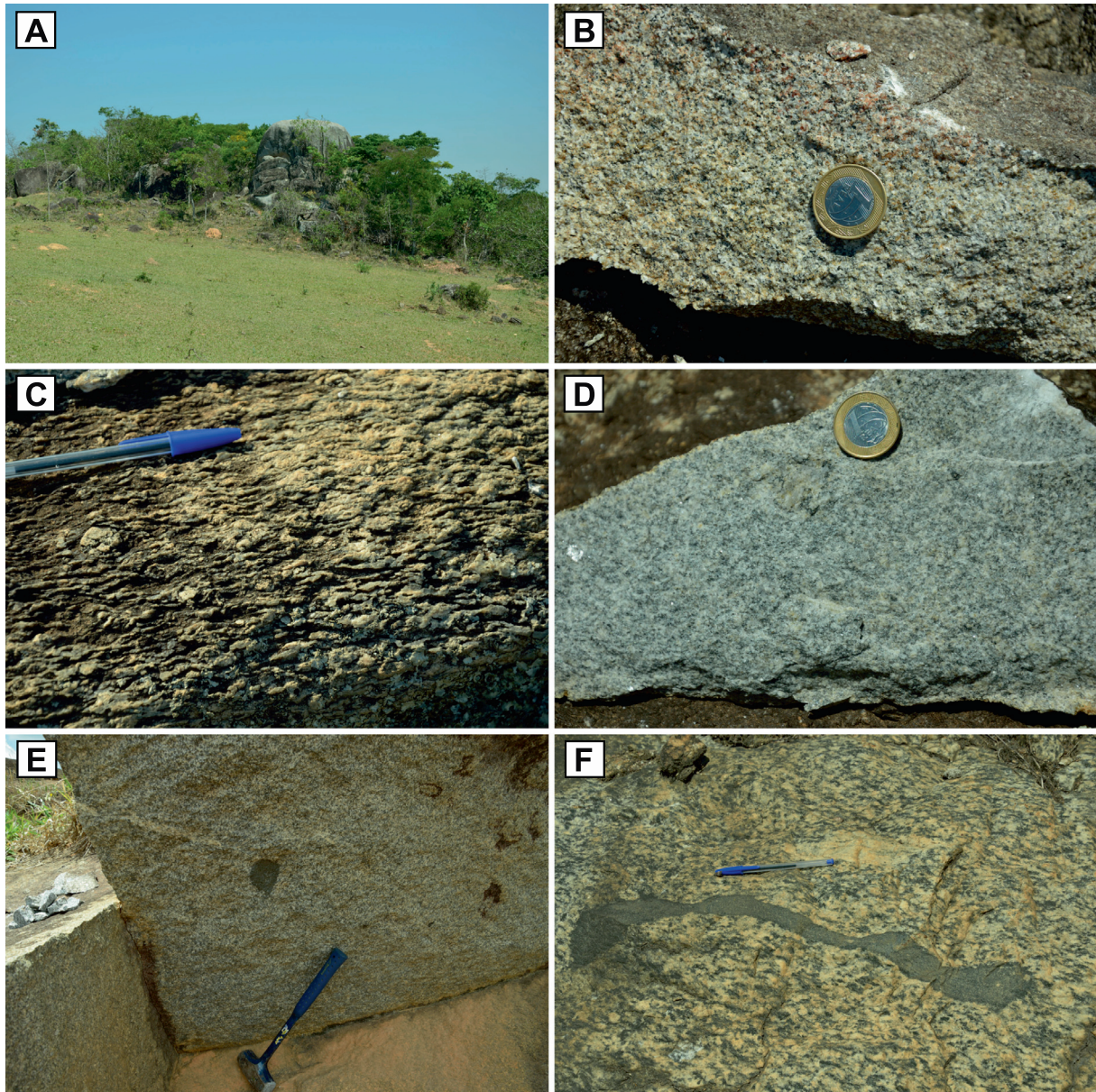


Fig. 2. Field photographs. (A) Panoramic view of various meter-scale blocks showing a typical outcrop of the Campo Belo granitoids (sample C-04). (B) Medium-grained equigranular biotite granite of the Rio do Amparo pluton (sample CB-09). (C) Hornblende-biotite orthogneiss that crops out within the Rio do Amparo pluton, showing subvertical mylonitic foliation (sample CB-23). (D) Medium-grained inequigranular biotite granite of the Bom Sucesso pluton (sample C-01). (E) Centimeter-scale biotite clots in the Bom Sucesso granite (sample CB-06). (F) Foliated coarse-grained Lavras granitoid (sample B-13) showing a decimeter-scale fine-grained mafic enclave.

Bom Sucesso I facies by Quéméneur (1996). The main Bom Sucesso granitic body is also intruded by meta-mafic dikes of the Timboré and Lençóis systems (Carneiro et al., 2007). Another granitic body located to the south of Bom Sucesso city was considered to belong to the Bom Sucesso pluton by Campos (2004). This facies consists of a highly porphyritic biotite monzogranitic orthogneiss with a subvertical foliation trending E-W. This author obtained a TIMS U-Pb zircon age of 2753 ± 11 Ma for this granitic intrusion that has been considered the age of the Bom Sucesso pluton.

The Lavras pluton is an elongated body of c. 20 km long and up to 10 km wide located between the cities of Lavras and Nepomuceno (Fig. 1B) (Quéméneur, 1996). It consists of equigranular to porphyritic coarse-grained hornblende-biotite granodiorites and monzogranites that locally show a mylonitic foliation trending E-W, likely related to the Lavras shear zone (Fig. 1), which is probably linked to Neoproterozoic tectonics affecting the Andrelândia mega-sequence (Quéméneur, 1996). The major

mineral assemblage comprises plagioclase (30–35 vol%), alkali feldspar (20–30 vol%), quartz (20–30 vol%) and mafic aggregates of amphibole (up to 17 vol%) and biotite (4–5 vol%). Biotite can appear as single crystals or replacing amphibole. The accessory assemblage consists of abundant titanite, epidote and Fe-Ti oxides, as well as, allanite, zircon and apatite. The Lavras pluton commonly contains centimeter to decimeter-size enclaves of quartz-feldspathic gneisses and meta-mafic rocks (Fig. 2F) (Trouw et al., 2008). It is crosscut by meta-mafic dikes of the Lençóis system, and by pegmatites and leucogranite dikes (Trouw et al., 2008). It is also intruded by the Porto Mendes granite to the northwest that is a light gray medium- to fine-grained, predominantly isotropic, biotite monzogranite (Noce et al., 2000) with an age of ca. 1976 Ma (Trouw et al., 2008). The Lavras granitoid pluton also intrudes the Campos Gerais TTG rocks (Trouw et al., 2008) and the Ribeirão Vermelho charnockite for which the documented U-Pb age is 2718 ± 13 Ma.

3. Samples and methods

We have studied 27 samples amongst which 6 samples are of the Rio do Amparo granite; 3 samples of hornblende-biotite orthogneiss enclaves from the Rio do Amparo pluton; 10 samples of the Bom Sucesso granite; 1 sample of a highly porphyritic biotite orthogneiss from the pluton located to the south of Bom Sucesso city; 6 samples of the Lavras granitoid; and 1 sample of a leucocratic dike intruding the Lavras granitoid in the vicinity of Nepomuceno city. The geographic coordinates of all samples are listed in Table 2. Whole-rock major and trace element compositions were determined for 26 samples, 6 samples were also analyzed for Nd isotopes (Tables 2 and 3). For U-Pb zircon analyses, zircon grains were separated from 12 samples of the different granitoids of the complex (Table 1 and Supplementary material).

3.1. Geochronology

All samples were crushed with a jaw crusher and powdered to approximately 300 μm . Heavy mineral concentrates have been obtained by panning and were subsequently purified using Nd-magnets, a Frantz magnetic separator and methylene iodide. Zircon grains were mounted in 1 inch round epoxy mounts resin, polished using diamond paste, and cleaned using 10% v/v HNO_3 followed by de-ionized water. Subsequently, the zircon grains were studied by cathodoluminescence imaging (CL). Isotope data were acquired on an ICP-MS Element XR (Thermo Scientific), coupled with an Excite193 (Photon Machines) laser ablation system, equipped with a two-volume HelEx ablation cell at the Institute of Geosciences of the University of Campinas (IG-UNICAMP). The acquisition protocol adopted was: 30 s of gas blank acquisition followed by the ablation of the sample for 60 s in ultrapure He (laser frequency at 10 Hz, spot size of 25 μm , and laser fluence of 4.74 J cm^{-2}). Data were collected for masses 202, 204, 206, 207, 208, 232, 235 and 238 using the ion counting modes of the SEM detector, except for masses 232 and 238, which were analyzed in combined ion counting and analogue mode. Four points were measured per mass peak, and the respective dwell times per mass were 4, 8, 4, 16, 4, 4, 4 e 4 ms. Data were reduced off-line using Iolite software (version 2.5) following the method described by Paton et al. (2010), which involves subtraction of gas blank followed by downhole fractionation correction comparing with the behavior of the 91500 reference zircon (Wiedenbeck et al., 1995). Peixe zircon standard (ID-TIMS age of 564 ± 4 Ma; cf. Dickinson and Gehrels, 2003) was used to monitor the quality of the reduction procedures. Common Pb correction was accomplished using Vizual Age version 2014.10 (Petrus and Kamber, 2012).

3.2. Whole-rock chemistry

3.2.1. Major and trace element compositions

Major and trace elements were analyzed on a Philips PW 2404 X-ray fluorescence spectrometer at the Institute of Geosciences of the University of Campinas (IG-UNICAMP), using fusion beads and pellets and following the procedures of Vendemiatto and Enzweiler (2001). Data quality was controlled routinely through analyses of the international reference rocks GS-N, DR-N, OU-6 and BRP-1; the relative errors for major and minor elements are 0.4–1.5%. The rare earth elements and other trace elements were analyzed on a Thermo (Xseries2) quadrupole ICP-MS at the Institute of Geosciences of the University of Campinas (IG-UNICAMP), following the in-house adapted analytical procedures of Eggins et al. (1997) and Liang et al. (2000), and instrument conditions of Cotta and Enzweiler (2009); the results have less than a 10% deviation from the recommended values for the international standard GS-N.

3.2.2. Nd isotopes

Nd isotope ratios were determined at the University of Granada by thermal ionization mass spectrometry (TIMS) with a Finnigan Mat 262 after high-pressure digestion using $\text{HNO}_3 + \text{HF}$ in Teflon-lined vessels and element separation with ion-exchange resins. All analytical procedure was performed using ultra clean reagents. Normalization value was $^{146}\text{Nd}/^{144}\text{Nd} = 0.7219$. Blank for Nd was 0.09 ng. The external precision (2σ), estimated by analyzing 10 replicates of the standard WS-E (Govindaraju et al., 1994), was better than $\pm 0.0015\%$ for $^{143}\text{Nd}/^{144}\text{Nd}$. $^{147}\text{Sm}/^{144}\text{Nd}$ ratios were directly determined by ICP-MS at the University of Granada following the method developed by Montero and Bea (1998), with a precision better than $\pm 0.9\%$ (2σ).

4. Zircon dating

Zircon grains of the Campo Belo granitoids tend to be metamictic and in some cases show elevated common lead. At least 100 zircon grains of each sample were studied by cathodoluminescence, from which we have used the least metamictic and discordant grains. The complete U-Pb data set is given in the Supplementary material. A summary of the U-Pb ages determined in this study is listed in Table 1 along with data from the literature. Concordia and $^{207}\text{Pb}/^{206}\text{Pb}$ weighted average diagrams are shown in Figs. 3 and 4. $^{207}\text{Pb}/^{206}\text{Pb}$ lower intercepts of the studied samples tend to zero or rarely to Neoproterozoic ages but without geological meaning because of their large errors.

Table 1
Summary of geochronological data of the Campo Belo granitoids.

Sample	Rock unit	Technique	Age (Ma)	References
JC 1554	Bom Sucesso granite	Rb-Sr	2748 ± 60	[1]
JC 1589	Bom Sucesso granite	TIMS	2753 ± 11	[2]
N-239	São Pedro das Carapuças granite	TIMS	2585 ± 51	[2]
CB-09	Riberao Vermelho Charnockite	LA-ICP-MS	2718 ± 13	[3]
CB-20	Rio do Amparo granite	LA-SF-ICP-MS	2716 ± 6	This study
CB-02	Rio do Amparo granite	LA-SF-ICP-MS	2693 ± 16	This study
CB-23	Hornblende-biotite orthogneiss	LA-SF-ICP-MS	2729 ± 4	This study
C-06	Hornblende-biotite orthogneiss	LA-SF-ICP-MS	2726 ± 4	This study
CB-05	Hornblende-biotite orthogneiss	LA-SF-ICP-MS	2727 ± 7	This study
15WEJE-9	Bom Sucesso granite	LA-SF-ICP-MS	2696 ± 6	This study
B-10	Porphyritic biotite orthogneiss	LA-SF-ICP-MS	2748 ± 5	This study
B-11A	Lavras granitoid	LA-SF-ICP-MS	2646 ± 5	This study
B-11B	Lavras granitoid	LA-SF-ICP-MS	2647 ± 5	This study
	Peraluminous leucogranitic dike	LA-SF-ICP-MS	2631 ± 4	This study

[1] Quéméneur (1996); [2] Campos and Carneiro (2008); [3] Trouw et al. (2008).

Table 2

Representative whole rock compositions of granitoids from the Campo Belo complex. Major elements in weight percent. Trace elements in ppm.

Sample	CB02	CB03	CB04	CB05	CB06	CB09	CB10	CB11	CB12	CB18	15WEJE2A	CB20	CB22	CB23	B10	B11A	B11B	B34	B13	C6	C5	C4	C3	C2	C1	B35
Rock Unit ^a	HBO	BSG	BSG	BSG	BSG	RAG	RAG	RAG	RAG	BSG	LG	RAG	RAG	HBO	LG	LG	Dike	LG	LG	HBO	BSG	BSG	BSG	BSG	BSG	LG
UTM	482396	529306	528948	527078	518254	492247	492253	491663	489574	524701	490753	490575	487450	498546	477294	478750	478750	478088	487945	527075	530451	528883	526253	526397	525926	495756
	7680670	7679094	7679104	7677381	7678431	7682254	7682260	7683401	7686142	7688497	7657079	7671427	7675839	7680184	7655760	7658916	7658916	7654590	7656874	7683857	7681725	7680587	7681770	7681392	7679446	7653827
SiO ₂	73.29	74.99	73.72	71.45	71.48	69.51	71.34	73.19	74.39	72.65	72.37	74.15	73.67	73.93	69.6	71.63	72.2	70.13	72.14	71.32	73.52	71.89	69.29	70.23	74.16	73.05
TiO ₂	0.495	0.201	0.249	0.521	0.506	0.417	0.267	0.101	0.112	0.243	0.56	0.083	0.075	0.372	0.512	0.347	0.034	0.579	0.539	0.593	0.402	0.47	0.578	0.54	0.232	0.468
Al ₂ O ₃	12.97	13.42	13.72	13.84	13.89	15.53	15.37	14.41	13.98	14.11	12.18	14.34	14.28	12.46	13.5	13.39	15.92	13.2	12.5	13.13	13.19	13.57	14.47	14.31	13.34	12.41
FeOt	3.15	1.31	1.76	2.75	2.6	2.2	1.54	1.09	0.99	1.86	3.74	0.78	0.8	2.77	4.68	3.22	0.33	4.45	3.66	3.64	2.37	2.59	3.12	2.9	1.37	3.26
MnO	0.04	0.014	0.035	0.028	0.022	0.025	0.013	0.015	0.009	0.023	0.048	0.014	0.017	0.047	0.073	0.033	0.003	0.049	0.043	0.04	0.03	0.028	0.03	0.03	0.023	0.039
MgO	0.43	0.31	0.44	0.68	0.64	0.63	0.42	0.21	0.16	0.43	0.51	0.11	0.23	0.23	0.19	0.15	0.06	0.25	0.4	1.23	0.41	0.6	0.64	0.58	0.39	0.36
CaO	1.42	0.99	1.34	1.51	1.59	1.16	0.84	0.78	1.09	1.15	1.72	0.74	0.73	1.34	1.78	1.3	1.31	1.5	1.68	0.93	1.25	1.51	1.8	1.38	1.07	1.54
Na ₂ O	3.36	3.19	3.63	3.3	3.37	4.05	3.76	3.45	3.82	3.44	3.32	3.48	3.43	3.36	2.94	2.56	4.35	2.84	3.62	3.23	3.6	3.3	3.32	3.25	3.22	3.46
K ₂ O	4.23	5.21	4.59	5.3	5.27	5.6	5.37	5.42	5.2	5.43	3.86	5.54	5.99	4.45	5.18	5.68	4.54	5.44	3.89	4.3	4.29	5.26	5.3	5.34	5.36	4.32
P ₂ O ₅	0.135	0.045	0.061	0.144	0.136	0.138	0.057	0.029	0.033	0.077	0.158	0.029	0.045	0.087	0.151	0.087	0.035	0.148	0.152	0.17	0.107	0.135	0.168	0.147	0.081	0.131
LOI	0.31	0.5	0.39	0.33	0.27	0.57	0.96	0.66	0.26	0.49	0.53	0.63	0.43	0.25	0.48	0.78	0.85	0.42	0.32	1.03	0.4	0.41	0.74	0.5	0.3	0.16
Total	99.83	100.18	99.94	99.86	99.77	99.83	99.94	99.35	100.04	99.91	99.00	99.9	99.7	99.3	99.08	99.18	99.63	99.00	98.95	99.61	99.57	99.76	99.46	99.2	99.54	99.2
Li		21.0	25.3	20.2		27.9			15.6	43.9		12.4	13.0	33.5	27.7	16.1	8.07	17.5	25.1	23.0	28.8	16.5	17.2	18.4	20.3	34.6
Be		1.98	2.79	1.80		1.74			0.99	2.18		1.97	1.35	3.38	2.04	2.52	1.51	2.69	2.72	2.54	2.33	1.9	1.54	1.59	2.00	3.04
Sc	6.00			5.72	4.00	2.80	3.00			2.73	4.00			1.67	5.50	2.10		3.83	3.93	6.46	5.59	4.87	6.36	5.65	1.71	4.90
V	24.6	9.10	14.4	23.9	28.9	18.6	15.3	7.40	6.94	13.6	27.0	11.0	11.2	10.7	3.40	4.00	4.66	5.20	22.6	26.5	21.7	20.7	23.0	23.8	11.6	17.9
Cr	7.70	8.60	7.80	18.3	19.2	11.9	6.70	4.50	12.6	26.8	18.2	8.88	24.4	14.4	8.80	3.60	9.95	7.70	18.7	10.8	34.5	21.5	21.5	15.5	18.3	17.6
Co		1.70	3.40	4.70		4.20			0.74	2.60		0.62	1.00	3.20	3.90	3.00	0.38	4.20	5.30	4.90	3.70	3.80	4.70	4.60	2.30	4.05
Ni	3.10	2.30	4.10	4.90	5.60	4.50	2.00	2.00	0.80	3.30	2.00	0.10	1.14	0.60		0.20	0.05	0.50	2.20	2.20	2.80	4.10	4.40	4.00	2.50	1.95
Cu	4.70	6.50	6.50	22.8	7.00	6.60	3.50	2.20	0.86	1.90	6.80	0.60	1.99	6.90	8.50	8.10	0.20	9.40	8.30	8.80	4.40	19.5	6.10	3.50	4.40	5.45
Zn	69.0	26.3	37.7	55.0	57.0	65.5	44.0	24.9	27.1	41.9	85.0	22.6	31.4	59.8	94.1	52.7	15.6	76.5	67.5	46.4	47.4	57.2	40.8	28.7	59.5	
Ga	16.7	16.6	18.1	19.3	16.4	21.8	19.1	18.2	15.3	19.1	15.2	15.4	15.0	19.2	22.3	22.1	17.6	22.8	17.9	21.3	20.2	19.2	21.2	21.1	16.9	19.1
Rb	163	245	247	215	164	224	155	149	132	267	107	164	172	138	106	126	109	124	70.7	116	330	213	213	234	280	176
Sr	135	105	128	161	168	248	240	153	96.5	146	159	149	214	61.1	114	50.6	476	64.6	94.9	79.8	91.4	119	127	111	106	116
Y	26.5	13.0	35.8	31.8	33.0	19.3	5.80	7.50	5.99	115	42.0	15.6	10.7	84.0	52.8	44.3	5.69	92.9	33.1	50.1	55.4	43.9	32.5	41.9	20.0	41.9
Zr	244	148	169	392	330	354	210	136	124.8	230	388	82.8	93.0	357	738	617	50.2	876	430	453	310	411	562	568	217	385
Nb	16.3	9.10	11.3	17.4	15.0	11.0	7.20	3.80	5.92	12.8	18.9	6.69	3.03	14.2	19.4	29.6	2.16	34.6	17.8	18.7	17.0	17.9	23.5	21.4	12.5	17.5
Mo		0.20	0.41	0.70		0.35			0.09	1.10		0.20	0.22	6.18	1.99	3.37	0.12	2.26	1.73	1.79	2.91	3.11	0.99	0.85	0.29	2.26
Sn		1.02	1.46	1.05		1.97			0.60	3.59		0.69	1.41	4.16	1.05	0.51	0.06	0.26	2.37	2.87	3.58	1.36	0.74	1.29	0.81	3.49
Cs		1.17	4.76	0.92		1.47			0.63	2.03		1.81	1.50	2.87	1.02	0.56	0.54	0.43	1.34	0.45	2.69	1.07	0.60	1.09	1.03	2.43
Ba	894	654	664	1175	1070	1713	1321	787	477	1212	1193	836	1281	999	2539	1886	1195	1860	1548	1456	834	1032	1219	1097	820	1140
La	52.0	23.2	80.9	136	110	215	115	28.0	25.1	115	47.0	45.4	40.6	103	61.5	106	18.9	76.8	32.4	69.0	162	120	169	125	51.6	79.3
Ce	142	51.9	130	226	190	281	128	43.0	44.5	189	117	53.1	75.7	90.2	90.1	113	94.3	144	69.8	131	274	209	314	308	145	157
Pr		4.90	14.8	25.1		29.6			4.48	19.0		8.87	8.23	17.9	12.7	20.8	3.59	16.6	8.00	13.0	27.8	21.5	31.8	24.9	10.4	15.1
Nd	41.0	15.4	49.1	79.1	74.0	87.4	46.0	11.0	13.8	59.9	50.0	27.7	24.7	63.9	48.5	70.7	10.9	61.5	30.5	46.5	88.8	102	80.9	33.9	51.3	
Sm		2.74	8.75	12.7		12.2			3.17	10.6		6.37	4.92	11.9	9.96	12.9	2.35	12.7	6.63	9.57	15.1	12.2	16.6	13.8	6.73	9.48
Eu		0.47	0.96	1.13		1.80			0.69	1.25		1.52	1.01	1.82	3.69	2.13	1.25	2.27	1.43	1.88	1.30	1.04	1.30	1.14	0.68	1.41
Gd		2.27	8.04	11.0		10.1			2.51	11.9		5.12	3.59	12.1	9.32	11.0	1.76	12.7	6.07	8.96	13.1	11.0	13.5	11.3	5.90	8.84
Tb		0.27	1.06	1.32		0.91			0.30	1.78		0.70	0.42	1.94	1.45	1.60	0.26	2.02	0.94	1.33	1.75	1.42	1.52	1.32	0.78	1.29
Dy		1.43	5.99	6.89		3.63			1.41	12.1		3.33	1.87	12.5	9.18	9.60	1.37	13.1	5.84	8.29	9.99	7.90	7.24	6.64	4.40	7.78
Ho		0.30	1.16	1.23		0.60			0.24	2.89		0.55	0.34	2.65	1.90	1.86	0.24	2.81	1.18	1.65	1.93	1.55	1.30	1.21	0.78	1.57
Er		0.88	2.93	3.08		1.52			0.61	8.66		1.41	0.96	7.36	5.11	4.78	0.66	7.56	3.17	4.38	5.04	3.97	3.09	3.04	1.91	4.17
Tm		0.13	0.39	0.40		0.16			0.07	1.37		0.16	0.12	1.11	0.77	0.69	0.08	1.06	0.48	0.65	0.71	0.55	0.38	0.37	0.24	0.62
Yb		0.68	2.21	2.28		0.88			0.44	7.55		1.06	0.86	6.78	4.98	4.32	0.61	6.21	3.05	4.01	4.29	3.14	2.15	2.04	1.33	3.90
Lu		0.12	0.34	0.32		0.13			0.07	1.23		0.15	0.13	1.02	0.79	0.63	0.09	0.92	0.46	0.60	0.60	0.48	0.31	0.30	0.19	0.58
Hf		4.63	5.16	10.2		9.87			4.17	7.00		2.60	2.89	9.93	16.4	15.6	1.73	21.0	10.7	10.5	8.40	10.7	13.9	14.4	6.59	10.2
Ta		0.55	0.50	0.59		0.38			0.20	1.61		0.40	0.30	0.81	0.93	0.78	0.16	1.22	0.91	1.20	1.12	0.63	0.67	0.73	0.48	1.17
W		1.49	1.45	1.86		1.90				2.39		0.04	0													

Table 3
Nd composition of Campo Belo granitoids.

Sample	Rock unit	Age for calculations (Ma)	¹⁴⁷ Sm/ ¹⁴⁴ Nd	¹⁴³ Nd/ ¹⁴⁴ Nd	Error Nd/Nd	¹⁴³ Nd/ ¹⁴⁴ Nd _i	εNd _i	T _{CHUR} (Ga)	T _{CR} (Ga)	T _{DM} (Ga)
B-10	Lavras pluton	2646	0.118	0.511142	0.002	0.509076	−2.52	2.89	3.19	3.06
CB-04	Bom Sucesso pluton	2696	0.107	0.510858	0.002	0.508959	−3.56	3.00	3.25	3.13
CB-05	Bom Sucesso pluton	2696	0.098	0.510732	0.003	0.508984	−3.08	2.93	3.18	3.06
CB-09	Rio do Amparo pluton	2716	0.085	0.510789	0.002	0.509272	3.12	2.5	2.78	2.66
CB-18	Bom Sucesso pluton	2696	0.103	0.511019	0.003	0.509188	0.93	2.62	2.92	2.79
CB-20	Rio do Amparo pluton	2716	0.124	0.511238	0.002	0.50901	−2.03	2.93	3.24	3.1
N-1*	Lavras pluton	2700	0.107	0.51103	0.008	0.509124	−0.19	2.72	3.01	2.88

* Sample N-1 taken from Trouw et al. (2008).

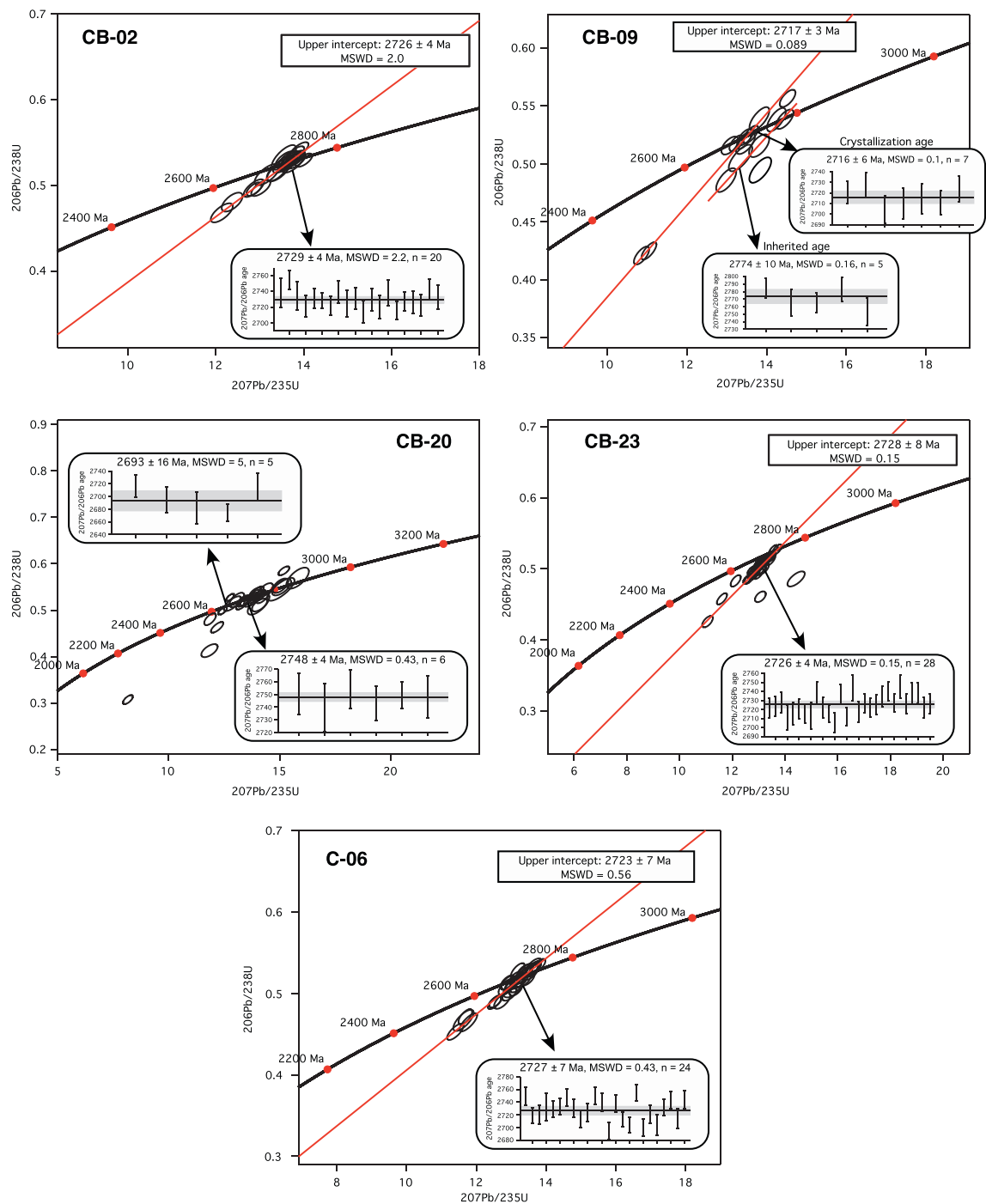


Fig. 3. Wetherill concordia plots for samples CB-02, CB-09, CB-20, CB-23 and C-06.

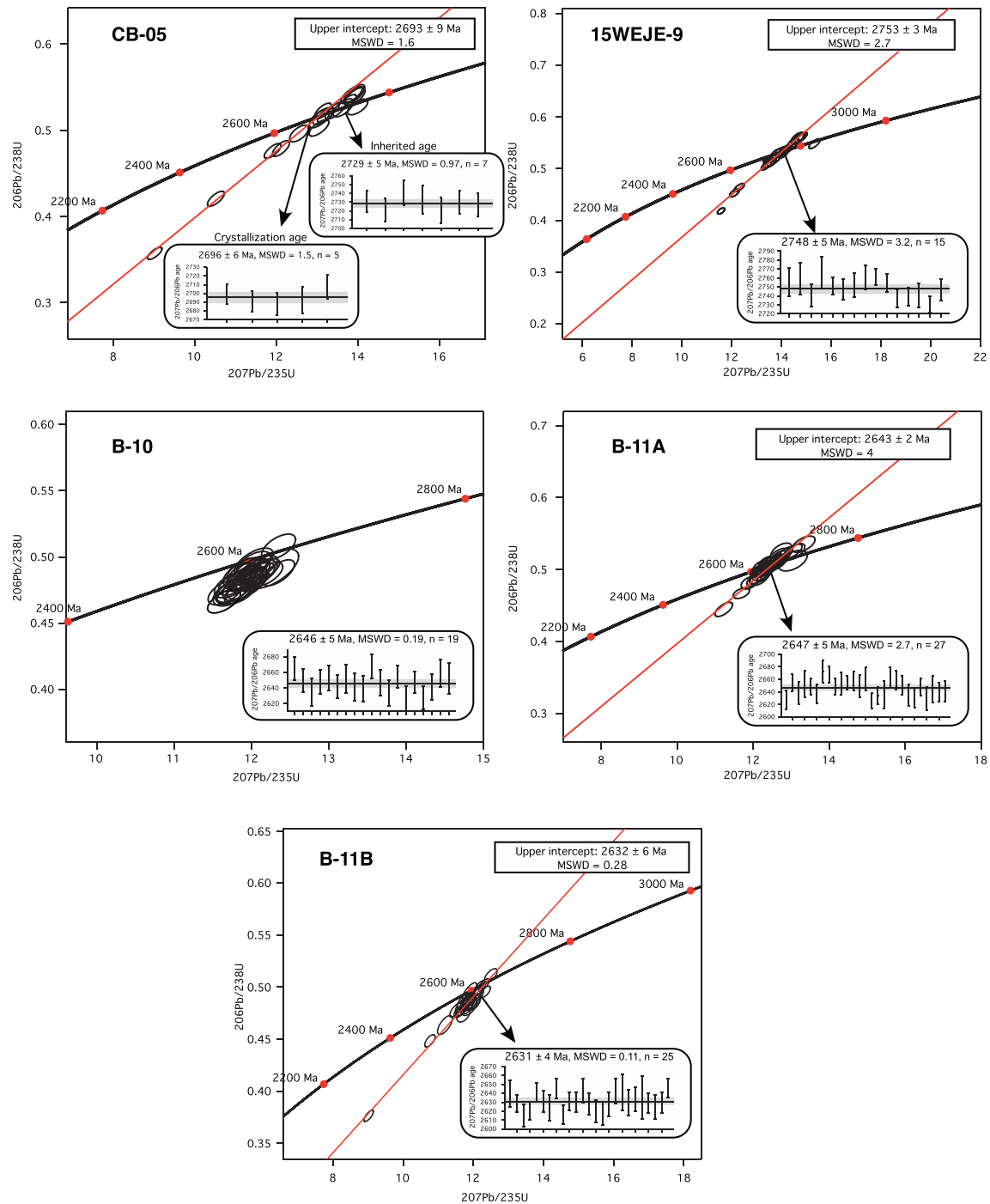


Fig. 4. Wetherill concordia plots for samples CB-05, 15WEJE-9, B-10, B-11A and B-11B.

In all samples, zircon grains are euhedral to subhedral, medium to long prismatic with pyramidal terminations that can be rounded and variable sizes around 70–300 μm long and 40–250 μm wide. Zircon grains can be brown, yellow and pink, translucent and opaque with zircons of the Lavras granitoid and the leucogranitic dike as well as those from the hornblende-biotite orthogneiss being mostly translucent and less metamictic. Some grains can show fractures and small irregular inclusions. Most grains exhibit oscillatory zoning although sector zoning is also common (Fig. 5).

4.1. Rio do Amparo pluton

We have studied two granite samples (CB-09 and CB-20) from the Rio do Amparo pluton. Sample CB-09 is an isotropic biotite granite, whereas sample CB-20 is a leucocratic granite.

Sample CB-09 presents two populations of zircon ages (Fig. 3), the younger shows a $^{207}\text{Pb}/^{206}\text{Pb}$ upper intercept of 2717 ± 3 Ma (MSWD = 0.089, $n = 9$) with a weighted mean $^{207}\text{Pb}/^{206}\text{Pb}$ age for the most concordant zircons (<2% discordance) of 2716 ± 6 Ma (MSWD = 0.1, $n = 7$) that may represent the crystallization age.



Fig. 5. Cathodoluminescence images and ages of selected zircons from the studied samples. See text for description.

On the other hand, the second population consists of inherited zircons with a $^{207}\text{Pb}/^{206}\text{Pb}$ upper intercept of 2777 ± 17 Ma (MSWD = 0.26, $n = 6$).

Most of the analyses in sample CB-20 were obtained from zircon cores because the rims are more metamictic. The interpretation of this sample is quite complicated as many subconcordant zircons fall on the concordia curve between 2693 and 2800 Ma. However, it can be inferred a possible $^{207}\text{Pb}/^{206}\text{Pb}$ crystallization age of 2693 ± 16 Ma (MSWD = 5, $n = 5$) that is very similar to that of sample CB-09 (2716 ± 6 Ma) within the error. This sample also has a high number of inherited zircons, six of them present a weighted $^{207}\text{Pb}/^{206}\text{Pb}$ mean age of 2748 ± 4 Ma (MSWD = 0.43, <3% discordance). Whereas, two older populations yielded the following $^{207}\text{Pb}/^{206}\text{Pb}$ ages: i) four zircons (<3% discordance) with ca. 2770 Ma and ii) seven zircons (<3% discordance, except two analyses that are 7% discordant) with ages between 2820 and 2880 Ma.

Given that the crystallization age of sample CB-20 is poorly constrained we consider the age of ca. 2716 Ma obtained for sample CB-09 as the best estimate of the crystallization age of the Rio do Amparo granite.

4.2. Hornblende-biotite orthogneiss

We have studied three samples (CB-02, CB-23 and C-06) of this granitic orthogneiss occurring as large inclusions in the Rio do Amparo pluton.

Samples CB-02, CB-23 and C-06 have weighted mean $^{207}\text{Pb}/^{206}\text{Pb}$ ages for the most concordant analyses of 2729 ± 4 Ma (MSWD = 2.2, $n = 20$, <5% discordance), 2726 ± 4 Ma (MSWD = 0.15, $n = 28$, <5% discordance) and 2727 ± 7 Ma (MSWD = 0.43, $n = 24$, <4% discordance), respectively. This suggests that the three samples belong to the same body, which crystallized around 2727 Ma.

4.3. Bom Sucesso pluton

Three samples of this pluton (CB-04, CB-05 and CB-18) have been studied, but zircons from samples CB-04 and CB-18 are very metamictic with very high contents of common Pb ($f^{206}(\%) > 5$ with most analyses ranging from 18 to 60), whereby it was not possible to obtain a meaningful age. Sample CB-05 is a medium-grained biotite syenogranite of the Bom Sucesso I facies.

Ten of the eighteen analyses of zircons from sample CB-05 yielded a $^{207}\text{Pb}/^{206}\text{Pb}$ upper intercept of 2693 ± 9 Ma (MSWD = 1.6) with a weighted mean $^{207}\text{Pb}/^{206}\text{Pb}$ age for the most concordant zircons (<2% discordance) of 2696 ± 6 Ma (MSWD = 1.5, $n = 5$), which is considered the best estimate of the crystallization age. The others are eight inherited zircons, seven of them with a weighted $^{207}\text{Pb}/^{206}\text{Pb}$ mean age of 2729 ± 5 Ma (MSWD = 0.97, <4% discordance) and one concordant analysis with a $^{207}\text{Pb}/^{206}\text{Pb}$ age of 2789 Ma.

4.4. Highly porphyritic biotite orthogneiss

One sample of the highly porphyritic biotite orthogneiss (15WEJE-9) that crops out to the south of Bom Sucesso city has been studied.

In sample 15WEJE-9 we performed 22 analyses on 20 grains, twenty of them gave a $^{207}\text{Pb}/^{206}\text{Pb}$ upper intercept of 2753 ± 3 Ma (MSWD = 2.7) with a weighted mean $^{207}\text{Pb}/^{206}\text{Pb}$ age for the most concordant zircons (<4% discordance) of 2748 ± 5 Ma (MSWD = 3.2, $n = 15$). This sample also has a concordant inherited zircon of ~ 2845 Ma. We therefore assume that the age of crystallization is 2748 ± 5 Ma.

4.5. Lavras pluton

We have studied two samples of coarse-grained hornblende biotite granitoid (B-10 and B-11A).

In sample B-10 we performed 35 analyses on 26 grains, all of them are concordant to subconcordant (<7% discordance) with a weighted mean $^{207}\text{Pb}/^{206}\text{Pb}$ age of 2656 ± 6 Ma (MSWD = 0.39). Taking into account the most concordant grains (<4% discordance) they gave a weighted mean $^{207}\text{Pb}/^{206}\text{Pb}$ age of 2646 ± 5 Ma (MSWD = 0.19, $n = 19$).

Sample B-11A has a $^{207}\text{Pb}/^{206}\text{Pb}$ upper intercept of 2643 ± 2 Ma (MSWD = 4, $n = 33$) with a weighted mean $^{207}\text{Pb}/^{206}\text{Pb}$ age for the most concordant zircons (<3% discordance) of 2647 ± 5 Ma (MSWD = 2.7, $n = 27$) and a concordant inherited zircon grain of ~ 2717 Ma.

Therefore the two samples belong to the same granitoid, which crystallized around 2646 Ma.

4.6. Leucocratic dike

One sample of a leucocratic plagioclase-rich biotite granitic dike (B-11B) that crosscuts the Lavras granite has been studied. 31 spots on igneous zircons reveal a $^{207}\text{Pb}/^{206}\text{Pb}$ upper intercept of 2632 ± 6 Ma (MSWD = 0.28) with a weighted mean $^{207}\text{Pb}/^{206}\text{Pb}$ age for the most concordant zircons (<4% discordance) of 2631 ± 4 Ma (MSWD = 0.11, $n = 25$), which is considered the crystallization age.

5. Whole-rock chemistry

5.1. Major and trace elements

The chemical compositions of the samples studied in this work are compared to previously published data of the Bom Sucesso and Lavras granitoids (Campos and Carneiro, 2008; Quémeuneur, 1996; Trouw et al., 2008) in the diagrams of Fig. 6.

All samples, except those from the southern Bom Sucesso body reported by Campos and Carneiro (2008), are high-silica granites ranging from 69.3 to 75.0 wt% SiO_2 (Fig. 6 and Table 2) showing mostly alkali-calcic and calc-alkalic compositions (MALI ($\text{Na}_2\text{O} + \text{K}_2\text{O} - \text{CaO}$ by weight) = 5.46–8.69; Fig. 6A). They are mainly alkaline in the sense of Sylvester (1989) (Fig. 6B) with samples of the Lavras pluton showing a stronger alkaline character. The Lavras

granitoid is clearly ferroan (Fe-number ($\text{FeOT}/(\text{MgO} + \text{FeOT})$ by weight) = 0.88–0.96) whereas the compositions of the Bom Sucesso and Rio do Amparo granites straddle the boundary between magnesian and ferroan compositions (Fe-number = 0.78–0.85 and 0.78–0.88, respectively); all of them plot in the compositional field of A-type rocks (Fig. 6C), although overlapping with the field of cordilleran high-silica granites is also shown (see further discussion in Section 6.3). The Rio do Amparo granite is peraluminous with normative corundum and some samples having ASI (alumina saturation index) index values higher than 1.1 (Fig. 6D), whereas the Bom Sucesso granite is slightly peraluminous with subordinate metaluminous compositions and the Lavras granitoid varies from metaluminous to slightly peraluminous (Fig. 6D). The highly porphyritic biotite granitoids from southern Bom Sucesso body reported by Campos and Carneiro (2008) show a clear different composition; they are strongly peraluminous and magnesian, high-silica granites (Fig. 6).

Trace element and REE concentrations (Table 2) are plotted, respectively, in Silicate Earth-normalized multi-element and Chondrite-normalized REE diagrams (Fig. 7). Chondrite-normalized REE-patterns are enriched in LREE compared to HREE ($(\text{La}/\text{Lu})_{\text{N}} = 9.70\text{--}76.7$, $32.5\text{--}171$ and $7.31\text{--}17.5$ for the Bom Sucesso, Rio do Amparo and Lavras granitoids respectively), with the Rio do Amparo granite showing the lowest HREE values (Fig. 7). Most samples exhibit a negative Eu anomaly ($\text{Eu}/\text{Eu}^* = 0.26\text{--}0.35$, $0.49\text{--}0.81$ and $0.47\text{--}0.69$ for the Bom Sucesso, Rio do Amparo and Lavras granitoids, respectively) although one sample of the Lavras pluton shows a small positive Eu anomaly ($\text{Eu}/\text{Eu}^* = 1.17$) that may most probably be caused by feldspar accumulation. Silicate Earth-normalized trace-element patterns are enriched in incompatible elements with negative Nb-Ta anomalies and a positive Pb anomaly (Fig. 7) suggesting crustal or subduction-related components in their source. The patterns also show negative Ba, Sr, P and Ti anomalies in all rock types except in the Lavras pluton (Fig. 7) for which most of the samples show a positive Ba anomaly. Despite the negative Ba anomaly, the three plutons present high Ba content (>500 ppm) with most samples of the Bom Sucesso and Lavras granitoids showing >1000 ppm Ba (Table 2). Ba and Sr are positively correlated in samples of the Rio do Amparo granite (Fig. 8A) whereas samples of the Lavras granitoid and the hornblende-biotite orthogneiss show an uncoupled Ba and Sr behavior (Fig. 8A). The Rio do Amparo and Bom Sucesso granites have very high Th and U values (Th: 21.3–104 ppm and U: 2.50–18.7 ppm). Their high Th content along with their high LREE contents result in Th/Nb, La/Nb and Ce/Pb ratios normalized to the Silicate Earth of 46.9–99.8, 4.31–19.8 and 0.06–0.50 for the Rio do Amparo pluton and 11.8–42.4, 2.59–9.66 and 0.14–0.82 for the Bom Sucesso pluton. On the other hand, the Lavras pluton has $(\text{Th}/\text{Nb})_{\text{N}}$, $(\text{La}/\text{Nb})_{\text{N}}$, and $(\text{Ce}/\text{Pb})_{\text{N}}$ ratios of 1.01–8.70, 1.85–4.61 and 0.27–0.46 respectively, which are within the range of the continental crust values ($(\text{Th}/\text{Nb})_{\text{N}} = 1.75\text{--}11.6$, $(\text{La}/\text{Nb})_{\text{N}} = 1.26\text{--}6.09$ and $(\text{Ce}/\text{Pb})_{\text{N}} = 0\text{--}0.45$; Moreno et al., 2016).

The mainly negative correlation of P_2O_5 and Zr with silica shown by all samples (Fig. 8B, C), indicate that the magmas were saturated in these elements and experienced fractionation of apatite and zircon.

Apatite-saturation temperatures (T_{Ap}) have been calculated following the thermometric expression developed by Harrison and Watson (1984), in which the temperature is calculated as a function of melt composition (SiO_2 content) and the distribution coefficient of P between apatite and melt (D_{P}). Correction proposed by Bea et al. (1992) for peraluminous compositions has been also used to avoid overestimated temperatures as a consequence of the elevated solubility of apatite in peraluminous granitic melts. Zircon-saturation temperatures (T_{Zr}) have been calculated according to the Watson and Harrison (1983) thermometric expression,

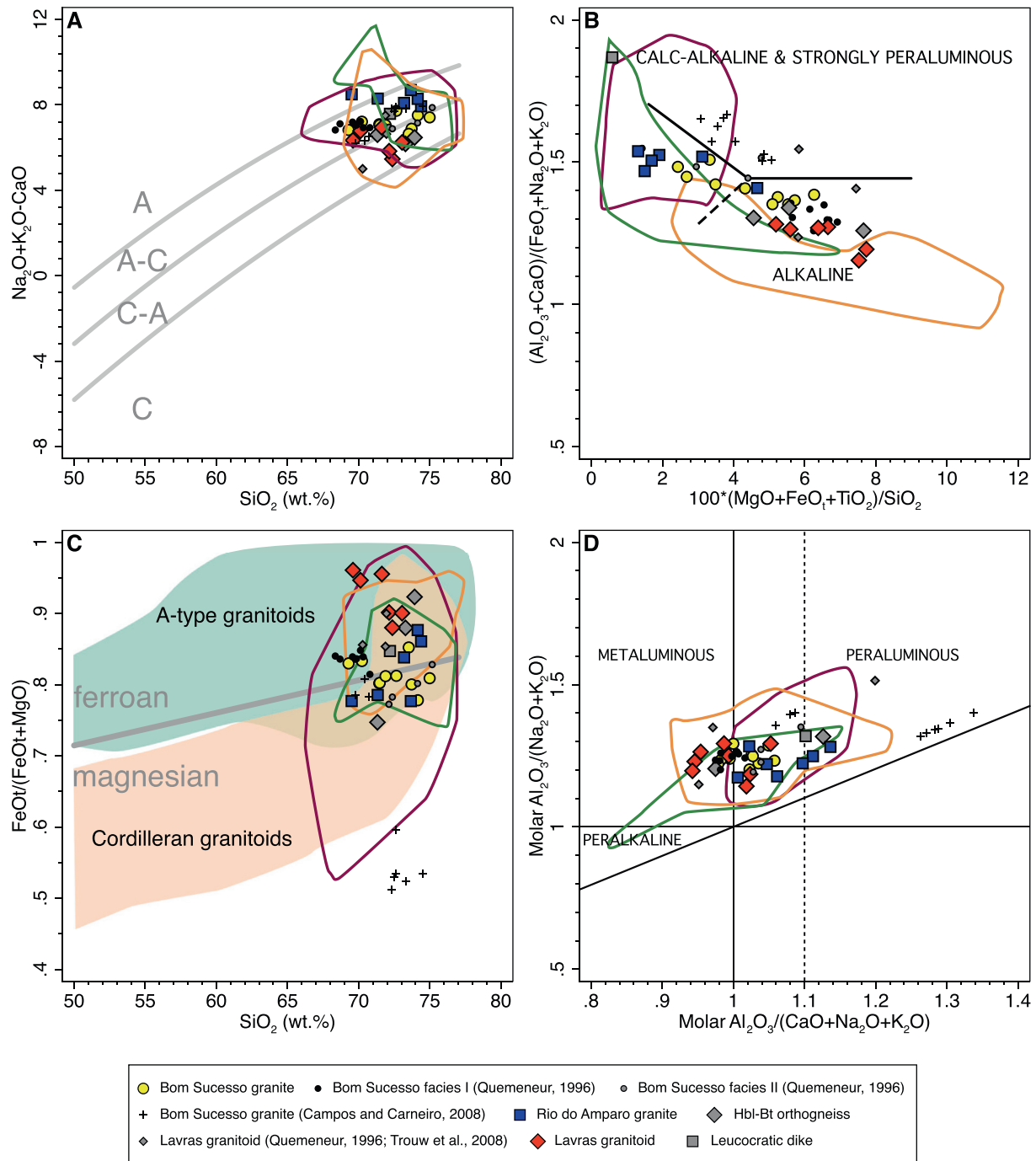


Fig. 6. Whole-rock composition of Campo Belo granitoids. (A) MALI-index vs. SiO_2 diagram (Frost et al., 2001). (B) Granite discrimination diagram of Sylvester (1989). (C) Fe-number vs. SiO_2 diagram. A-type and cordilleran granitoid fields after Frost et al. (2001). (D) Molar alumina saturation index vs. $\text{Al}_2\text{O}_3/(\text{Na}_2\text{O} + \text{K}_2\text{O})$. Compositions of high-K granitoids from the northern (orange lines) and southern (green lines) São Francisco Craton and the Congo Craton (purple lines) are shown for comparison. (For interpretation of the references to colour in this figure legend, the reader is referred to the web version of this article.)

based on the distribution coefficient of Zr between zircon and melt (D_{Zr}) and parameter $M = [(\text{Na} + \text{K} + 2\text{Ca})/(\text{Al} - \text{Si})]$, which is considered the best compositional proxy for zircon dissolution processes since zircon solubility strongly depends on magma composition (e.g., alkalinity, ASI).

All samples display relatively high T_{Ap} and T_{Zr} , being in general higher than 740 °C (Table 2). The results also indicate that T_{Ap} is generally about 50 °C higher than T_{Zr} , suggesting earlier apatite saturation. The Bom Sucesso and Lavras granitoids and the hornblende-biotite orthogneiss show temperatures higher than c. 800 °C, whilst the Rio do Amparo granite presents temperatures

between 740 and 840 °C with sample CB-09 showing temperatures as high as 898 °C.

5.2. Nd isotopes

Nd isotope compositions of the studied samples are listed in Table 3. The $^{147}\text{Sm}/^{144}\text{Nd}$ ratios of the analyzed samples are below the threshold value of 0.165 above which calculated model ages may be unreliable (Stern, 2002).

The studied rocks have mostly negative ϵNd_i values (Rio do Amparo: −2.0; Bom Sucesso: −3.6 and −3.1; Lavras: −2.5 and

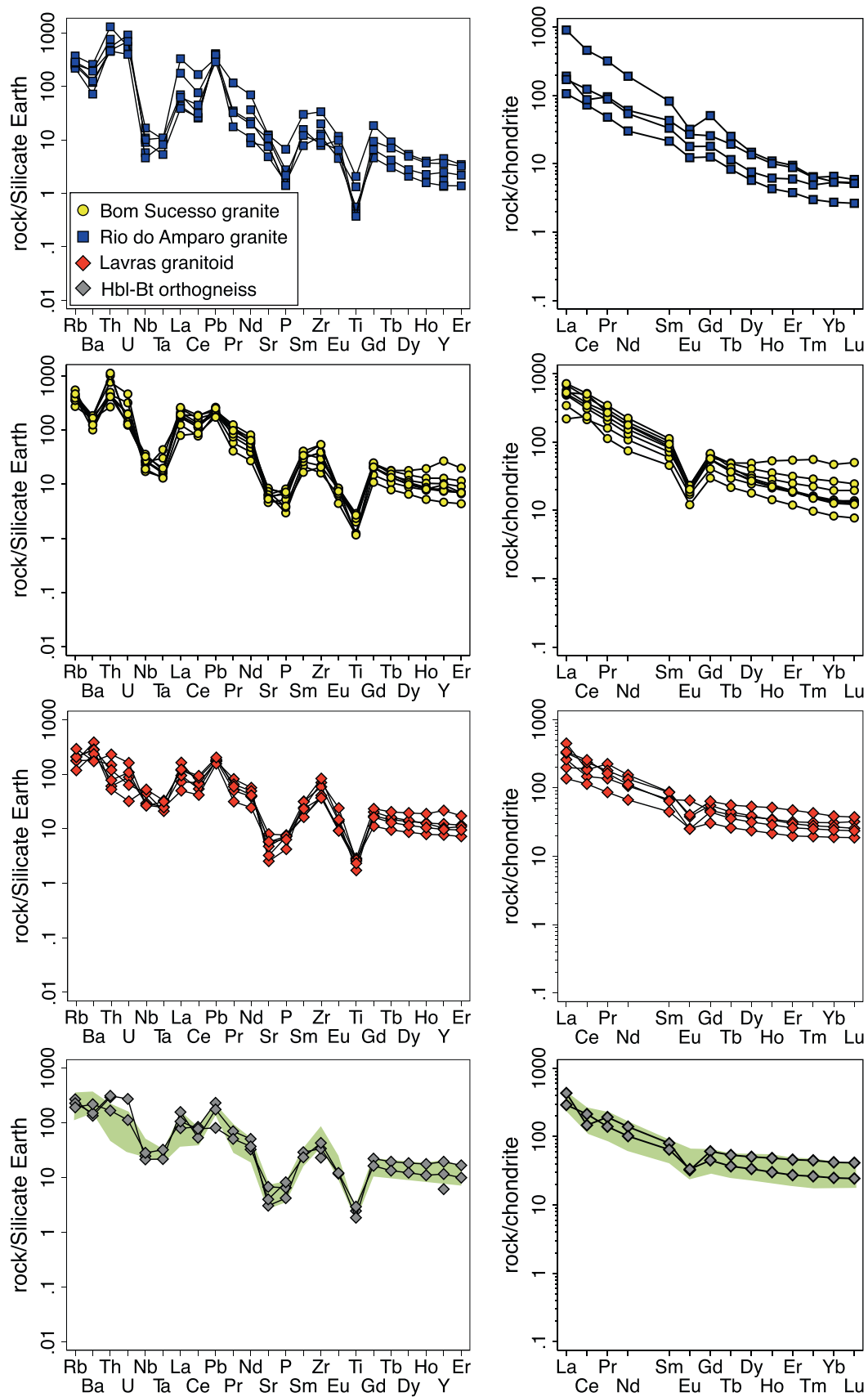


Fig. 7. Silicate Earth-normalized trace element and Chondrite-normalized REE diagrams. Normalization values after [McDonough and Sun \(1995\)](#). Green field shows composition of the Lavras granitoid for comparison with the hornblende-biotite orthogneiss. (For interpretation of the references to colour in this figure legend, the reader is referred to the web version of this article.)

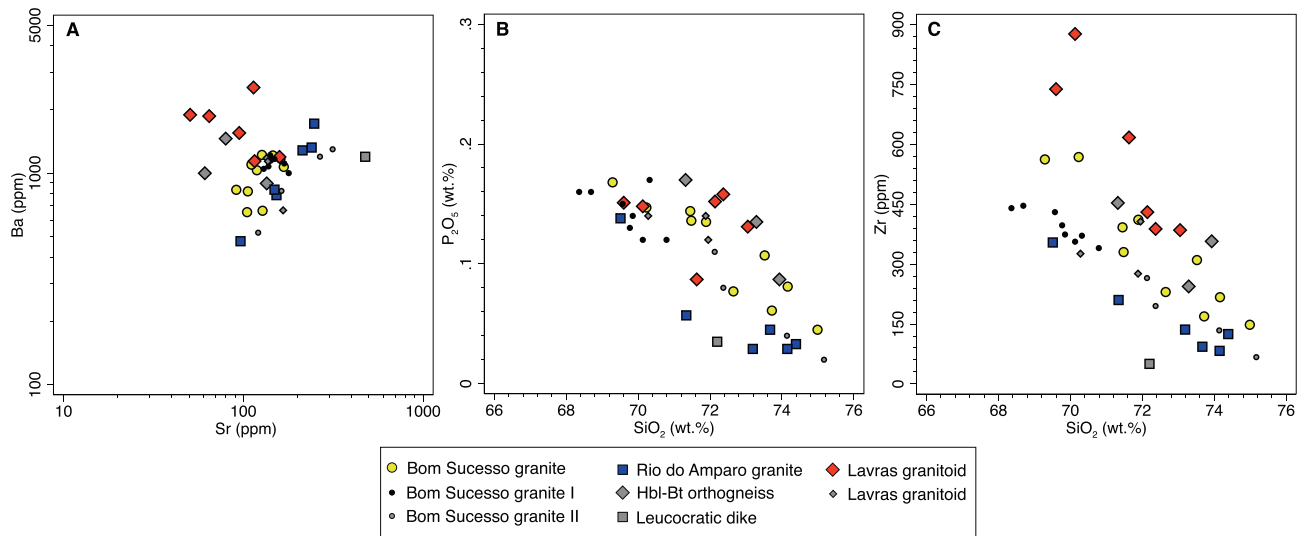


Fig. 8. Harker and Ba vs. Sr diagrams for Campo Belo granitoids. Major elements in wt(%) and trace elements in ppm. Small gray and black symbols are data from Quéméneur (1996) and Trouw et al. (2008).

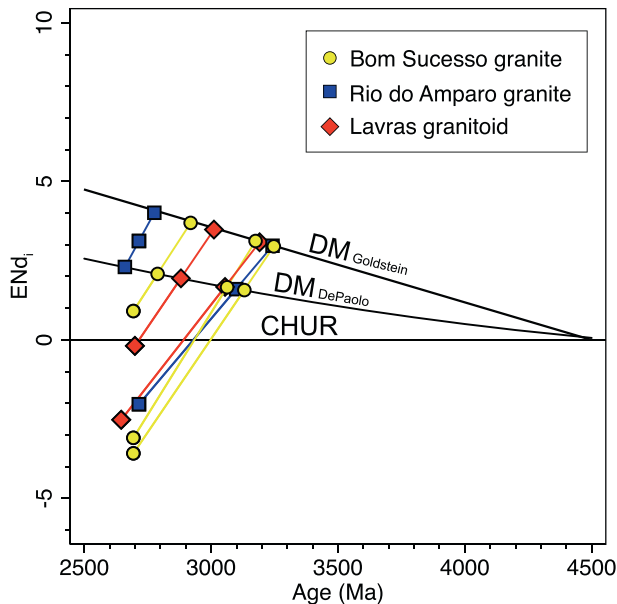


Fig. 9. ϵ_{Ndi} vs. U–Pb zircon ages with reference lines for depleted mantle (DM) after DePaolo (1981) and Goldstein et al. (1984) and Chondritic Uniform Reservoir (CHUR).

–0.2) with the exception of samples CB-09 and CB-18 with values of +3.1 and +0.9, respectively (Fig. 9 and Table 3). The Nd model ages (T_{DM} , calculated according to DePaolo (1981)) for most samples range between 3.06 Ga and 3.13 Ga that are significantly older than the U–Pb zircon ages (Table 3), whereas, Samples CB-09 from Rio do Amparo, CB-18 from Bom Sucesso and N1 from Lavras show a juvenile character with T_{DM} varying between 2.66 and 2.88 Ga.

6. Discussion

6.1. Sequence of emplacement of the Campo Belo granitoids

Comparison of the ages obtained here with those from the literature permit to clarify relationships between the different high-K granitoids of the complex, which are essential for further geochemical studies to better infer the petrogenesis of these complex rocks.

The crystallization age of 2716 ± 6 Ma obtained for the Rio do Amparo granite is much older than that of 2585 ± 51 Ma reported by Campos and Carneiro (2008) for a coarse-grained biotite-hornblende granite from the São Pedro das Carapuças pluton, traditionally ascribed to the Rio do Amparo pluton, which in turn is chemically different to the main Rio do Amparo pluton (see details in Campos, 2004 and Campos and Carneiro, 2008). We therefore, conclude that the two intrusions represent two different granitic bodies. On the other hand, the age of ca. 2727 Ma (2729 ± 4 Ma, 2726 ± 4 Ma and 2727 ± 7 Ma) of the hornblende-biotite orthogneiss included in the Rio do Amparo pluton is almost the same that the age of the Rio do Amparo pluton (ca. 2716 Ma), indicating that both are coeval or, perhaps the hornblende-biotite orthogneiss slightly older. Furthermore, they are also different mineralogically and chemically (see Sections 5.1 and 6.3). They may therefore represent mega-enclaves of country rocks to the Rio do Amparo pluton as proposed for the occurrences of the Ribeirão dos Motas meta-mafic-ultramafic layered-sequence into the Candeias and Itapeçerica migmatitic gneisses and the Rio do Amparo pluton (Carneiro et al., 2007).

The highly porphyritic biotite orthogneiss that crops out to the south of Bom Sucesso city has a crystallization age of 2748 ± 5 Ma that is identical to the TIMS U–Pb age of 2753 ± 11 Ma reported by Campos and Carneiro (2008), which in addition has been considered the age of the Bom Sucesso pluton. However, the remarkably younger age of 2696 ± 6 Ma obtained here for the Bom Sucesso facies I along with the difference in geochemistry between the two rocks (see Section 5.1) indicates that the highly porphyritic biotite orthogneiss must represent the country rock to the Bom Sucesso pluton.

The crystallization age of ca. 2646 Ma (2646 ± 5 Ma and 2647 ± 5 Ma) of the Lavras granitoid is in contrast with the conclusion reached by Trouw et al. (2008). These authors have suggested the Lavras granitoid to be older than the Ribeirão Vermelho charnockite (2718 ± 13 Ma; Trouw et al., 2008), based on the existence of xenoliths of quartz-feldspathic orthogneiss, mineralogically and texturally similar to the Lavras granitoid, in the charnockite. Nevertheless, the younger ages of the Lavras pluton presented here suggest that this granitoid intruded the Ribeirão Vermelho charnockite and thus that the xenoliths occurring in the latter should belong to another granitoid.

Another interesting point that emerges from the ages we have obtained, is that, contrarily to a previous assessment (see Trouw

et al., 2008 and references therein), the Rio do Amparo and Lavras granitoids are two different plutons. This is also supported by differences in petrography and geochemistry (see Sections 5.1 and 6.3).

Summarizing, the geochronological data presented in this work and those reported from literature for the Campo Belo metamorphic complex (CBMC) suggest that migmatitic TTG gneisses from the Fernão Dias gneiss (migmatization event at 2.84 Ga; Teixeira et al., 1998) were intruded by different high-K granitoid plutons between 2.75 and 2.63 Ga.

The metaluminous hornblende-biotite orthogneiss that appears as enclaves within the Rio do Amparo pluton, and the peraluminous highly porphyritic biotite orthogneiss exposed to the south-east of Bom Sucesso city were emplaced at 2727 and 2748 Ma, respectively. The presence of a penetrative foliation trending E-W in both granitoids suggest a deformation event between 2750 and 2720 Ma prior to the intrusion of the undeformed Rio do Amparo biotite granite at 2716 Ma. Afterwards, the Bom Sucesso biotite granite, essentially undeformed as emphasized by Quéménéur (1996), and the Lavras hornblende-biotite granitoid were emplaced at 2696 Ma and 2646 Ma, respectively. The intrusion of the peraluminous leucogranitic dikes at 2631 Ma marked the end of the Archean magmatism in the CBMC. The local E-W mylonitic foliation developed on the Lavras hornblende-biotite granitoid suggests that the shear zone that crosses the boundary between the CBMC and the Andrelândia mega-sequence is younger than 2646 Ma that is consistent with a Neoproterozoic age for the amalgamation of them as suggested by Quéménéur (1996) and Trouw et al. (2008).

The long time span, from 2750 to 2630 Ma, of high-K granitoid magmatism in the CBMC revealed here fits well with previous published data of granitoids from the southern and northern São Francisco Craton that evidence a major episode of high-K granitoid magmatism between 2760 and 2600 Ma (Cruz et al., 2012; Farina et al., 2015a; Lopes, 2002; Machado and Carneiro, 1992; Machado et al., 1992; Marinho et al., 2008; Noce et al., 1998; Romano et al., 2013; Santos-Pinto et al., 2012). In fact, the main granitic plutons in the CBMC formed between ca. 2730 and 2650 Ma may correspond to the Mamona event (2760–2680 Ma) described by Farina et al. (2015a) in the Bonfim and Bação complexes, which mainly consists of weakly deformed to undeformed granite plutons that may locally develop prolate $L > S$ fabric and occasionally be highly foliated showing an augen-gneiss structure (Farina et al., 2015a, 2015b; Romano et al., 2013). Interestingly, the apparent lack of Paleoproterozoic deformation affecting the Neoproterozoic high-K granitoids from the southern São Francisco Craton (SSFC) is supported by the preservation of titanites of Neoproterozoic age and the absence of Paleoproterozoic metamorphic zircons (Aguilar et al., 2017). This contrasts with the Neoproterozoic high-K granitoids reported from the northern São Francisco Craton (NSFC) that were deformed and metamorphosed by Paleoproterozoic events (Cruz et al., 2012; Santos-Pinto et al., 2012), suggesting a differential behavior of both sectors of the craton in the Paleoproterozoic.

Romano et al. (2013) pointed out that the main peak of granitic magmatism in the SSFC took place between ca. 2750 and 2700 Ma with a volumetrically minor event at ca. 2612 Ma (Noce et al., 1998; Romano et al., 2013). Nonetheless, the ages of the Campo Belo granitoids reveal younger granitic magmatism at 2650 and 2630 Ma (Lavras granitoid and leucogranitic dikes respectively) that has not been previously reported in the SSFC. Granitoids of 2.66–2.65 Ga have been also described in the northern sector of the craton (Lopes, 2002; Marinho et al., 2008), which therefore indicate a similar magmatic evolution in both the northern and southern segments of the craton.

Crystallization ages between 2720 and 2666 Ma, very similar to those of the Campo Belo granitoids, have been reported from metaluminous to slightly peraluminous biotite granites with subordinate amphibole and clinopyroxene from the Ntem Complex in the Congo Craton (Shang et al., 2010; Tchameni et al., 2000). These granites are undeformed although they can be locally affected by shear zones, similarly to the high-K granitoids of the Mamona event from the SSFC. The timing of the high-K granitoid magmatism enhances the similarities between the Congo and São Francisco cratons, which have been commonly correlated by reason of the direct connection between the cratons before drifting of Africa from South America and their similar evolution during the Archean and Paleoproterozoic (e.g., Cordani, 2003; Cordani et al., 2009; De Waele et al., 2008).

6.2. Zircon inheritance

This study points out to a differential zircon inheritance between the high-K granitoids of the Campo Belo complex. On the one hand, the Rio do Amparo and Bom Sucesso granites present a high proportion of inherited zircons, being close to 40% of the analyzed zircons in each sample. The Rio do Amparo granite presents different populations of inherited zircons with ages of ~2750 Ma, 2770–2790 Ma and 2820–2880 Ma, being that of 2770–2790 Ma the most representative one, whereas the Bom Sucesso granite has a significant population with an age of ~2730 Ma along with one zircon grain of ~2789 Ma. On the other hand, inherited zircons are absent or scarce in the highly porphyritic biotite orthogneiss (one zircon grain of ~2845 Ma), the hornblende-biotite orthogneiss, the Lavras granitoid (one zircon grain of ~2717 Ma) and the peraluminous leucogranitic dike.

Geochronological data of high-K granites from Belo Horizonte, Bonfim and Bação complexes reported by Romano et al. (2013) and Farina et al. (2015a) indicate that inherited zircons are normally absent in such granites and in the few cases in which inheritance has been observed the cores have ages close either to 2780 Ma and to 2900 Ma. Furthermore, published data of Neoproterozoic granitoids from the NSFC also suggest a relatively low amount of inherited cores for such rocks although ages around 2960 Ma have been described (Cruz et al., 2012; Santos-Pinto et al., 2012). On the other hand, reported TIMS data of zircons from granitoids from the Congo Craton also indicate the existence of inherited zircons with ages around 2780 Ma (Shang et al., 2010).

The available data seem to suggest therefore that the zircon inheritance in the Rio do Amparo and Bom Sucesso granites is not only higher than in the rest of the Campo Belo granitoids but also higher than in other high-K granitoids from the southern and northern São Francisco Craton (Cruz et al., 2012; Farina et al., 2015a; Romano et al., 2013; Santos-Pinto et al., 2012). Zircon survival can be a consequence of that the temperature achieved by the magma is not high enough to dissolve zircon grains or that the kinetics of the magma prevent zircon dissolution (Bea et al., 2007). The Campo Belo granitoids have similar compositional parameters ($M = 1.31\text{--}1.52$, $ASI = 0.98\text{--}1.13$ for samples with geochronological data) and temperatures ($>800^\circ\text{C}$) high enough to dissolve zircon grains, which do not support the contrasting behavior of these granitoids. Other possibilities to account for this distinctive behavior may be either shielding by major phases that host accessory minerals (Bea, 1996a) or differences in heat transfer and magma cooling rates (Bea et al., 2007) between the various granitoids. The main major mineral that host zircon crystals is biotite (Bea, 1996a) whereby, in this case, preservation of inherited zircons by shielding can be ruled out because biotite is present as an early phase in all rocks types of the complex and thus, a similar inheritance should be expected. Therefore the differential inheritance

detected in the Campo Belo granitoids might be more probably related to variations in the kinetics of heat move to and from the various magmas (Bea et al., 2007), resulting in differing cooling rates that may favor or prevent zircon dissolution.

On the other hand, contrary to what suggested by whole-rock Nd data with T_{DM} mostly varying between 3.0 and 3.4 Ga (Cruz et al., 2012; Santos-Pinto et al., 2012; Shang et al., 2010; Tchameni et al., 2000), reported zircon ages seem to indicate a major involvement of crust formed at 2770–2790 Ma with none or scarce involvement of crust older than 2.9 Ga in the generation of Neoproterozoic high-K granitoids in both the São Francisco and Congo cratons (Cruz et al., 2012; Farina et al., 2015a; Romano et al., 2013; Santos-Pinto et al., 2012; Shang et al., 2010). Gneisses and granitoids older than 2.8 Ga also present low proportion of zircon grains with ages >2.9 Ga (Albert et al., 2016; Farina et al., 2015a; Lana et al., 2013), suggesting either that the juvenile sources of 3.0–3.4 Ga were zircon poor which point to rather mafic sources or that the zircon grains were dissolved in the 2.8 Ga magmatic event. Therefore, subsequent partial melting of the ca. 2.8 Ga sources that formed by reworking of previous crust and have scarce inherited zircons (Albert et al., 2016), may explain the discrepancy between the T_{DM} and the age of the inherited zircon grains of the 2.75–2.6 Ga high-K granitoids.

6.3. Geochemical characterization of the Campo Belo high-K granitoids

The moderately magnesian to ferroan character along with the alkaline affinity (Fig. 6), and high $Na_2O + K_2O$ (Fig. 10A) of the Campo Belo granitoids studied here suggest an A-type affinity (see Eby, 1990 and Frost and Frost, 2011 for further discussion). Accordingly, their compositions mostly plot in the field of within-plate granites in the tectonic discriminating diagrams of Verma et al. (2013) (Fig. 10B) and most samples from Bom Sucesso and Lavras plutons and the hornblende-biotite orthogneiss show the characteristic enrichment in HFSE and LREE of A-type granites (Fig. 10A). However, most samples of Rio do Amparo granite are more depleted in HFSE and LREE with values similar to those of I- and S-type granites; but, they are much more enriched in Th (Fig. 11) with values typical of A-type granites, and show significantly high Th/Nb ratios when compared to active continental and ocean island arcs data compiled by Moreno et al. (2016) (Fig. 12). Remarkably, the Rio do Amparo granite also presents higher Th/Nb values than the worldwide Proterozoic and Phanerozoic A₂-type granitoid database compiled by Moreno et al. (2014) (Fig. 12A). In accordance with an A-type character, apatite- and zircon-saturation temperatures of the Bom Sucesso and Lavras granitoids and the hornblende-biotite orthogneiss as well as the least evolved samples of the Rio do Amparo granite are significantly high with values higher than 800 °C.

The origin of A-type granites is still highly debated and they either may have been generated from mantle-derived magmas, partial melting of lower crust or mixing of these two end-members (see more details in Bonin, 2007). All samples mostly plot in the field of A₂-type granites (Fig. 13) in the discriminating diagrams of Eby (1992) and in Fig. 12A. They are therefore A-type granites with element ratios similar to continental crust or to subduction-related magmatism (Eby, 1990, 1992; Moreno et al., 2014, 2016). Regarding Nd isotopes, the negative ϵ_{Nd_i} values together with Nd model ages close to 3.1 Ga corroborate the significant reworking of Mesoproterozoic crust in the Campo Belo granitoids previously indicated by Teixeira et al. (1998). However, the involvement of juvenile material is also suggested by slightly negative (–0.2) and positive (+3.1 and +0.9) ϵ_{Nd_i} values and Nd model ages ranging between 2.7 and 2.9 Ga, which suggest the involvement of mantle and crustal sources in the generation of the three plutons.

Nature of magma sources can be also discriminated by trace elements ratios such as Y/Nb, Th/Nb, La/Nb and Ce/Pb, which are sensitive to mantle and crustal sources (Moreno et al., 2014, 2016, and references therein). The A₂-type affinity along with the relationships of Y/Nb, Th/Nb, La/Nb and Ce/Pb ratios suggest a crustal and/or subduction-related mantle source for the Lavras granitoid and the hornblende-biotite orthogneiss (Fig. 12). However, the Bom Sucesso and Rio do Amparo granites plot outside the continental crust and subduction-related magmatic fields (Fig. 12) because of their strong enrichment in Th and LREE relative to Nb. Samples with the highest Th abundances also present superchondritic Nb/Ta values that are extensive to all the Campo Belo granitoids (Fig. 14) and that more likely seem to suggest involvement of a TTG crustal source (Green, 1995; Hoffmann et al., 2011).

Granitoids with elevated Th and LREE contents must derive from Th-LREE rich sources because metaluminous liquids tend to have the same Th abundance as the source, whereas peraluminous sources normally produce segregates markedly poorer in Th (Bea, 2012). Because monazite is a major Th and LREE carrier in granites (Bea, 1996b), the generation of high-Th granitoids have been explained by preferred monazite dissolution during partial melting of monazite-bearing crustal sources (Stepanov et al., 2012) or by derivation from crustal sources previously metasomatized by mantle-derived supercritical alkaline fluids that would also favor monazite dissolution (Bea et al., 2001; Martin, 2006; Montero et al., 2009; Moreno et al., 2012). However, these mechanisms can hardly explain the high-Th abundance of the Campo Belo granitoids because it should be expected a pronounced negative Eu anomaly (Bea and Montero, 1999; Montero et al., 2009). This difficulty may be solved if Th-orthosilicates (huttonite-thorite) with limited monazite substitution were involved in the source region. Fertilization-type reactions, which have been proposed as a mechanism of fertilization of refractory intermediate to mafic sources of A-type granitoids (Martin, 2006), by F-rich alkaline fluids could favor Th-orthosilicate dissolution via generation of HFSE-fluoride complexes (Keppler and Wyllie, 1991; Keppler, 1993). High fluorine contents reported for high-Th A-type granitoids from the Caraguatá suite by Cruz et al. (2012) (range: 120–3268 ppm) support this mechanism.

6.4. Comparison with other Neoproterozoic high-K granitoids from the São Francisco and Congo cratons

High-K granitoids from Bonfim and Bação complexes from the SSFC, which range from granodiorite to syenogranite and leucogranite (Carneiro et al., 1997; Farina et al., 2015a), are similar to those from Campo Belo in terms of major element compositions. They range from metaluminous to mildly peraluminous and are mainly ferroan with subordinate magnesian compositions, and alkali-calcic to calc-alkalic (Fig. 6) except the Brumadinho granite from the Bonfim complex that presents distinctive alkalic compositions. Most samples from Bonfim and Bação complexes plot in the compositional field of alkaline and highly fractionated calc-alkaline granites in the discrimination diagram of Sylvester (1989) (Fig. 6B), but samples from the Mamona batholith (Bonfim complex) that show a clear alkaline affinity and samples from leucogranitic sheets in the Bação complex that are calc-alkaline granitoids (Fig. 6B). Granitoids from the Bação complex have lower REE and HFSE than the Campo Belo granitoids, whereas most samples from the Bonfim complex present LREE, Th and Nb contents close to those of the Bom Sucesso granite and similar or slightly lower Zr abundances. The alkaline and ferroan character of many samples from the Bonfim complex as well as their Zr + Nb + Ce + Y contents higher than 350 ppm (Whalen et al., 1987) and their enrichment in Y relative to Nb (Fig. 13) suggest an A₂-type affinity. However,

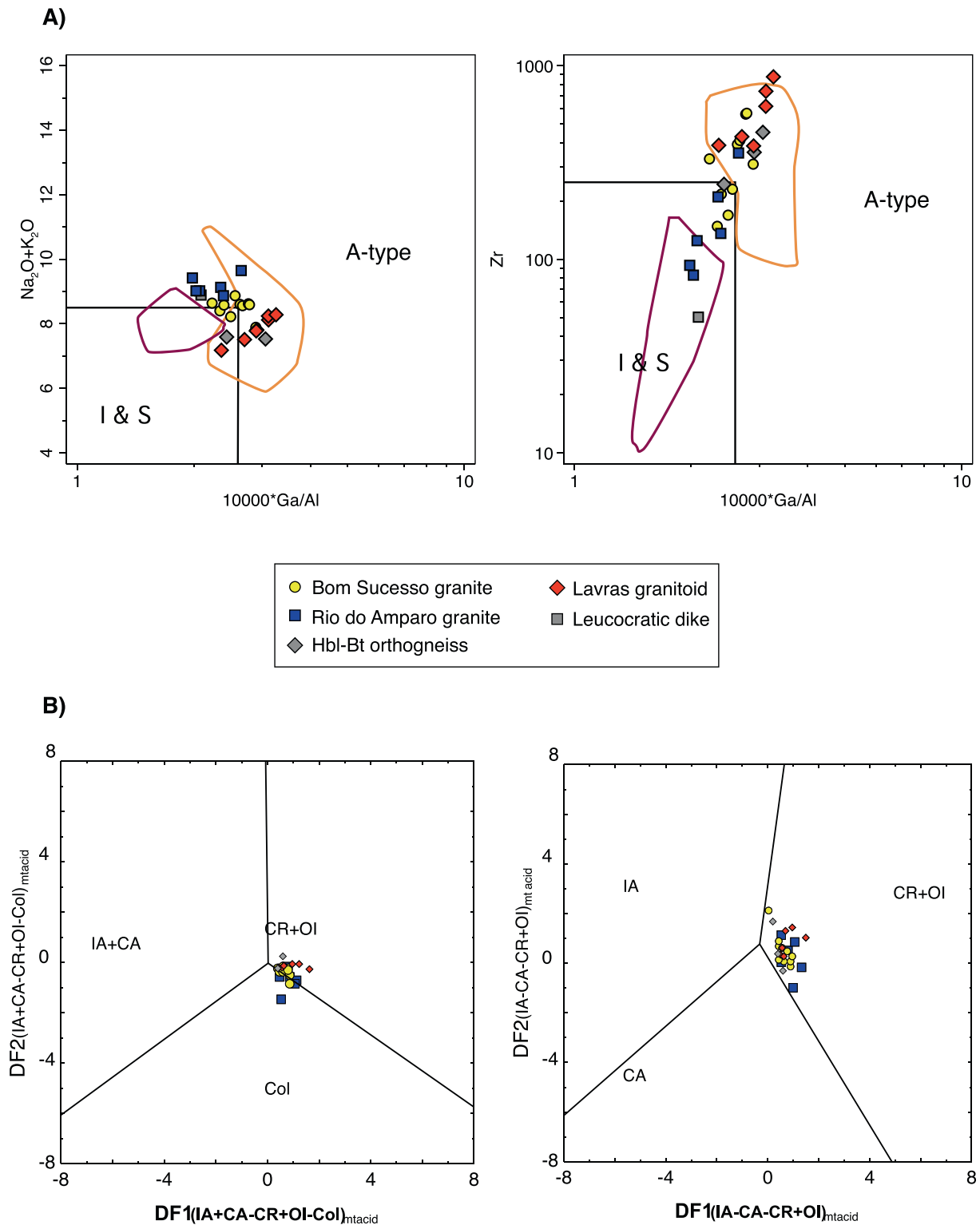


Fig. 10. (A) Granitoids discrimination diagrams from Whalen et al. (1987) for Campo Belo granitoids. Compositions of high-K granitoids from the northern São Francisco Craton (orange lines) and the Congo Craton (purple lines) are shown for comparison. (B) Tectonic discriminating diagrams from Verma et al. (2013) for Campo Belo granitoids. Abbreviations: CA, Continental Arc; Col, Collision; CR, Continental Rift; IA, Island Arc; OI, Ocean Island. (For interpretation of the references to colour in this figure legend, the reader is referred to the web version of this article.)

granitoids from the Bação complex seem to show an I-type affinity. In both complexes, $(Y/Nb)_N$ values are similar to those of the Campo Belo granitoids whereas $(Th/Nb)_N$ values from most samples are comparable to those of the Lavras pluton and these from some samples from the Bonfim complex are similar to those of

the Bom Sucesso pluton (Fig. 12). On the other hand, granitoids from both complexes have highly variable $(Ce/Pb)_N$ and $(La/Nb)_N$ (Fig. 12) values reaching significantly lower values than in the Campo Belo granitoids, plotting outside the compositional arrays defined by OIB-Subduction-related magmatism (Fig. 12).

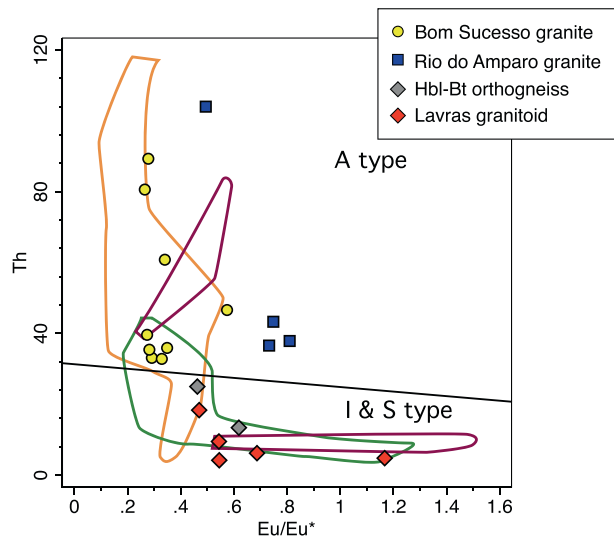


Fig. 11. Th vs. Eu/Eu^* diagram. Fields for A-type and S- and I-type granites after Eby (1992). Orange, green and purple lines represent data from northern and southern São Francisco Craton and the Congo Craton respectively. (For interpretation of the references to colour in this figure legend, the reader is referred to the web version of this article.)

Orthogneisses from the NSFC range from syenite to granite and are metaluminous to peraluminous and clearly ferroan and alkaline with compositions comparable to those of the Lavras pluton (Fig. 6; Cruz et al., 2012; Santos-Pinto et al., 2012). They are enriched in Ba and Zr with contents similar to those of the Bom Sucesso and Lavras plutons (Fig. 10A), and show very high LREE contents that match those of the Bom Sucesso pluton and the least evolved samples of the Rio do Amparo pluton. Their Th contents are very high with values even higher than those of the Rio do Amparo granite (Fig. 11). Moreover, they are richer in Nb and Y than the Campo Belo granitoids. Cruz et al. (2012) have suggested an A₂-type affinity for the orthogneisses of the NSFC (Fig. 13). They present $(\text{Th}/\text{Nb})_{\text{N}}$ and $(\text{Y}/\text{Nb})_{\text{N}}$ ratios comparable to those of the Bom Sucesso and Lavras plutons supporting their A₂-type character. Notably, in six samples of orthogneiss with available Pb data, the $(\text{Ce}/\text{Pb})_{\text{N}}$ values are higher than one (Fig. 12), which is controversial with a continental crustal or subduction-related source (Moreno et al., 2014, 2016). This feature combined with a Silicate Earth negative Nb anomaly (Fig. 7 in Cruz et al., 2012) may be indicative of a carbonatite component in their source as proposed by Moreno et al. (2014, 2016) for Neoproterozoic A₂-type granitoids from the Sinai Peninsula (Egypt).

The northern sector of the Congo Craton, mainly composed of Archaean charnockites, greenstone formations and TTGs intruded by dolerite dykes and high-K granitoids, has been correlated with the SFC by many authors (e.g., Cordani, 2003; Cordani et al., 2009; De Waele et al., 2008). Archaean high-K granitoids that appear in the Ntem complex (northwestern margin of the Congo Craton; Shang et al., 2007, 2010; Tchameni et al., 2000) are granodiorites, monzogranites, syenogranites and leucogranites with peraluminous and alkaline to calc-alkaline compositions (Fig. 6). They can be highly ferroan like the Campo Belo granitoids, but also highly magnesian sharing characteristics of cordilleran-type granitoids. They have lower Zr (Fig. 10A) and LREE abundances than the Campo Belo granitoids, but variable Th contents (Fig. 11). They also have lower Nb contents ($\text{Nb} = 0.3\text{--}6$ ppm) than the Campo Belo granitoids—except two samples with Nb close to 25 ppm. Their compositions show no clear alkaline affinity in the diagram of Sylvester (1989) (Fig. 6B) in which they lie in the fields of calc-alkaline granites, and of highly fractionated I-type granites and

alkaline granites (Fig. 6B). According to these relationships, along with their cordilleran affinity (Fig. 6C)—note that the ferroan samples plot close to the overlapping fields of cordilleran and A-type granitoids—and their slightly peraluminous composition as well as their I-S-type affinity in the discrimination diagrams of Whalen et al. (1987) (Fig. 10A) suggest an I-type affinity. On the other hand, their $(\text{Th}/\text{Nb})_{\text{N}}$ values are comparable to those of the Bom Sucesso granite (Fig. 12) besides three samples that match the Rio do Amparo values. They have $(\text{Y}/\text{Nb})_{\text{N}}$, $(\text{La}/\text{Nb})_{\text{N}}$ and $(\text{Ce}/\text{Pb})_{\text{N}}$ ratios comparable to those of the Campo Belo granitoids (Fig. 12). Accordingly, these trace element ratios along with the I-type affinity of the Ntem complex granitoids suggest derivation from a crustal or subduction-related source.

Our study reveals the existence of Archaean A-type magmatism in the SSFC as in the northern part of the craton (e.g., Cruz et al., 2012) and probably in the Bonfim complex (Carneiro et al., 1997; Farina et al., 2015a). In contrast, no Neoproterozoic A-type magmas have been described so far in the Congo Craton (Shang et al., 2010; Tchameni et al., 2000).

High-K granitoids from the northern São Francisco Craton and the Congo Craton exhibit εNd_i ranging between -3.0 and -6.0 , and between -2.5 and -5.3 respectively, which correspond to T_{DM} of $3.1\text{--}3.5$ Ga and $3.0\text{--}3.4$ Ga (Cruz et al., 2012; Marinho et al., 2008; Santos-Pinto et al., 2012; Shang et al., 2010; Tchameni et al., 2000). Because of this, its generation has been commonly linked to recycling of a Paleoproterozoic–Mesoproterozoic crust. In the same way, Albert et al. (2016) suggested a crustal origin for granites from the Bonfim and Bação complexes that belong to the Mamona event, since they have εHf_i values varying between -1 and -6 and elevated $\delta^{18}\text{O}_{(\text{Zrn})}$ ($>6.5\text{‰}$). Accordingly, most samples of the Campo Belo granitoids present T_{DM} of ca. 3.1 Ga and εNd_i ranging from -2.0 to -3.6 , which are similar or slightly less negative than those of granitoids from the northern São Francisco and Congo cratons. Similarly, the ca. 2.7 Ga Brumadinho granite from the Bonfim complex with εNd_i of -0.96 and -2.75 and T_{DM} of 2.9 and 3.1 Ga (Carneiro et al., 1997) also suggest participation of old Mesoproterozoic crust along with a younger crustal component. However, three samples of this study with εNd_i ranging from -0.2 to $+3.1$ and younger T_{DM} values (range: $2.7\text{--}2.9$ Ga) suggest that a more juvenile source could also be involved in the genesis of the Campo Belo granitoids. This is supported by εHf_i data in detrital zircons from the SSFC (Albert et al., 2016) that suggest that around 20% of the magmatism generated at ca. 2700 Ma must have been juvenile. Therefore, it seems that there is no evidence of the participation of a juvenile component in the source of the Neoproterozoic high-K granitoids from the NSFC and the Congo Craton, whereas contribution of a juvenile component in the source of SSFC granitoids is suggested by whole-rock Nd and zircon Hf isotopes.

Interestingly, in the case of the Rio do Amparo pluton the least evolved sample (CB-09) shows a clear juvenile character with positive εNd_i ($+3.1$) and T_{DM} of ca. 2.7 Ga, which is close to the crystallization age (~ 2716 Ma) and the age of the main population of inherited zircons found in this sample (~ 2777 Ma). This suggests recycling of new crust formed around 2780 Ma, probably of TTG affinity given its superchondritic Nb/Ta ratio. By contrast, sample CB-20 has negative εNd_i (-2.0), T_{DM} of 3.1 Ga and a higher number of inherited zircons with ages varying between 2750 and 2880 Ma, either suggesting reworking of older crust or assimilation of country rocks. Different degrees of assimilation of country rocks, either sedimentary or igneous, could explain the elevated number of inherited zircons with a wide range of crystallization ages in sample CB-20. Accordingly, the Rio do Amparo granite shows a subhorizontal trend in the MALI diagram (Fig. 6A) changing from alkaline to more calcic compositions as silica increases that is consistent with assimilation of small amounts of partial melts derived from peraluminous and calc-alkaline host rocks (Frost and Frost, 2008). Such

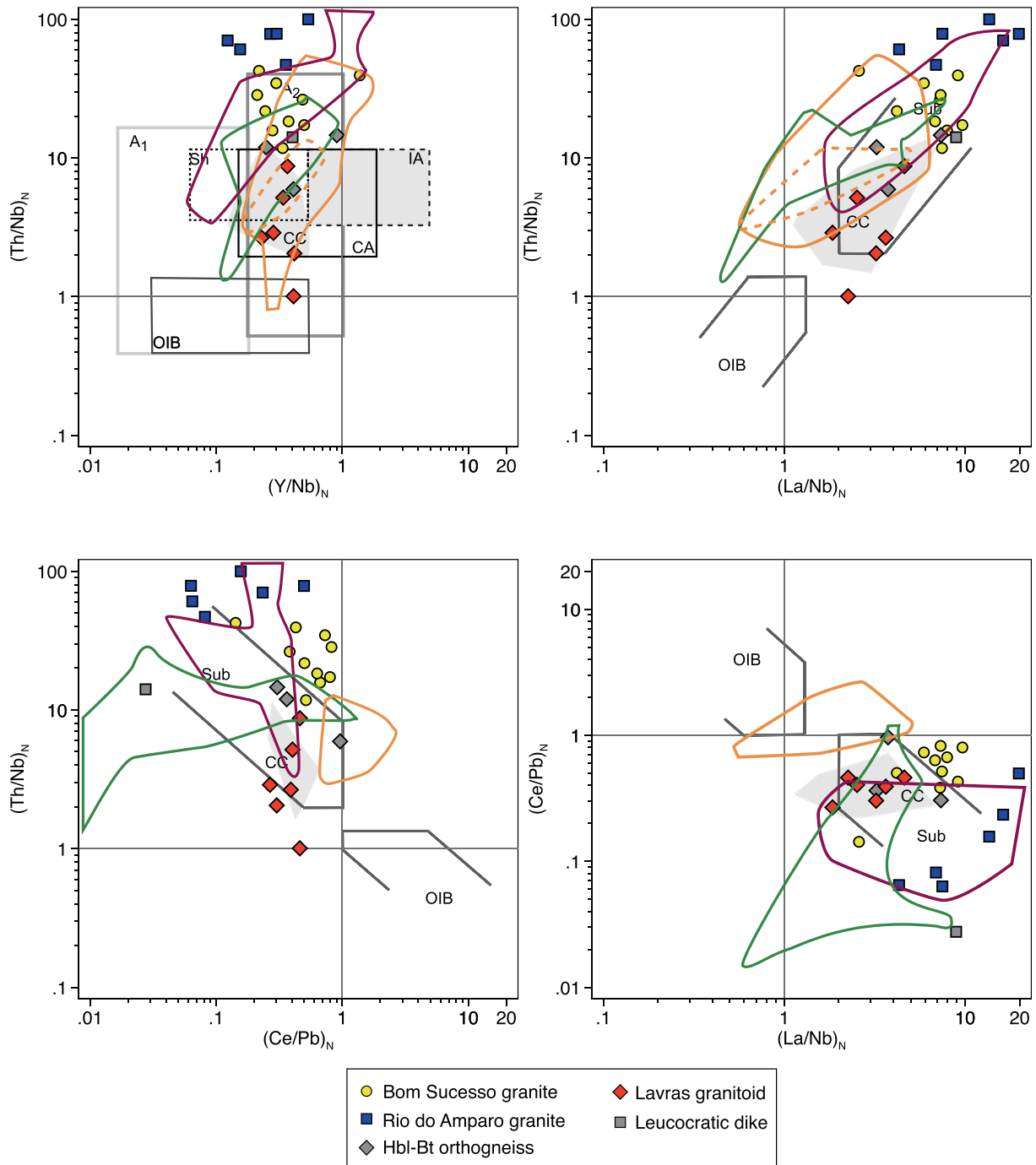


Fig. 12. Relationships between Y/Nb, Th/Nb, La/Nb and Ce/Pb in Campo Belo granitoids. Normalization values after McDonough and Sun (1995). Compositional fields after Moreno et al. (2016). Abbreviations: A₁, A₁-type granitoids; A₂, A₂-type granitoids; CA, Continental Arcs; CC, Continental Crust; IA, Island Arcs; OIB, Ocean Island Basalts; Sh, shoshonites; Sub, subduction-related magmatic suites. Compositions of high-K granitoids from the northern (orange lines) and southern (green lines) São Francisco Craton and the Congo Craton (purple lines) are shown for comparison. Orange dashed line in the $(Th/Nb)_N$ vs. $(Y/Nb)_N$ and $(Th/Nb)_N$ vs. $(La/Nb)_N$ diagrams depicts samples from northern São Francisco Craton with Pb data. (For interpretation of the references to colour in this figure legend, the reader is referred to the web version of this article.)

assimilation processes can modify the magma to a more peraluminous composition as observed in the Rio do Amparo granite. The contaminant component should be comparatively depleted in Ba and Sr to explain their positive correlation (Fig. 8A). Consequently, the Rio do Amparo granite could have been generated by partial melting of an igneous source formed at ca. 2780 Ma, probably related to the Rio das Velhas II magmatic event (2800–2760 Ma; Lana et al., 2013), with varying degree of host rock assimilation.

6.5. Tectonic setting and intercontinental correlations

Granitoids from the Campo Belo metamorphic complex (CBMC) mostly plot in the fields of continental rift and ocean island magmatism (Fig. 10B) in the discrimination diagrams of Verma et al. (2013). This feature is typical of A-type granitoids (Eby, 1992), which can be generated in post-collisional and within-plate tectonic settings. The A₂ type affinity of the Campo Belo granitoids, even those without significant isotopic crustal signature, suggests

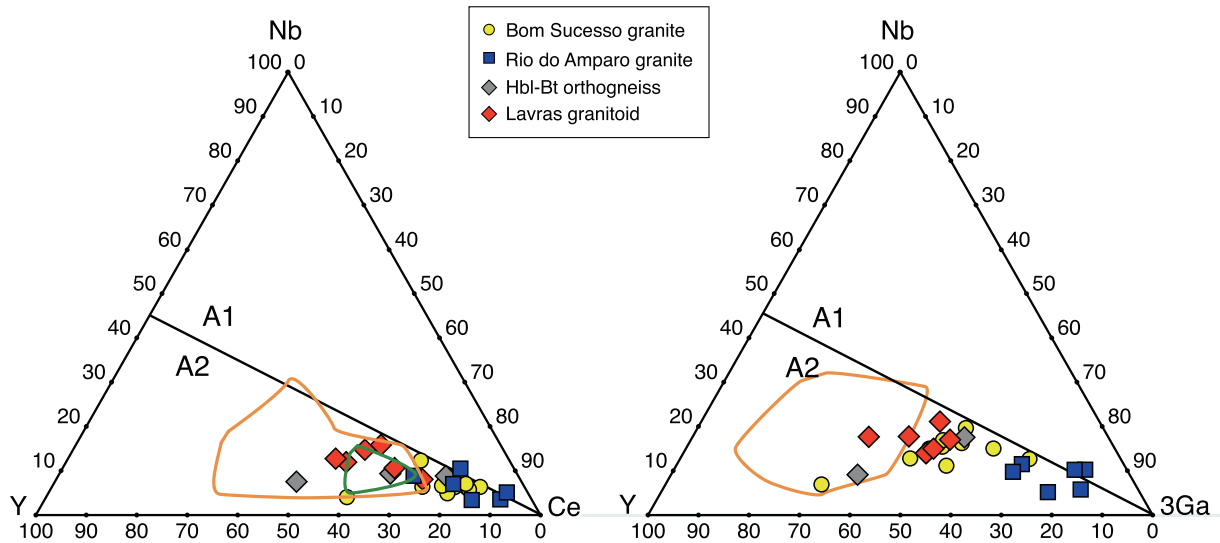


Fig. 13. A-type granitoids discrimination diagrams of Eby (1992) for Campo Belo granitoids. Orange and green lines show compositions of A-type granitoids from the northern São Francisco Craton and the Bonfim complex (southern São Francisco Craton) respectively. (For interpretation of the references to colour in this figure legend, the reader is referred to the web version of this article.)

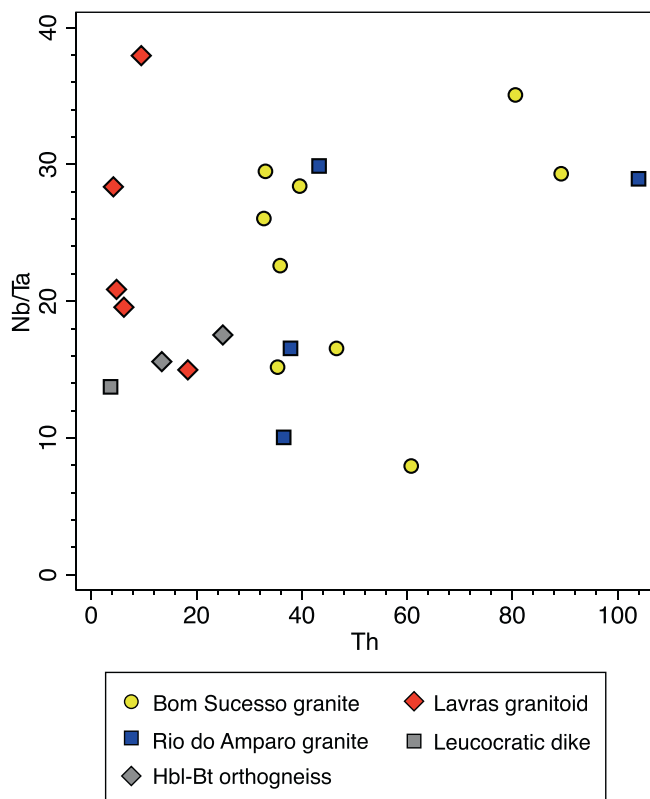


Fig. 14. Nb/Ta vs. Th diagram for Campo Belo granitoids.

generation from sources originally formed by subduction or continent–continent collision but does not permit to discriminate between post-collisional or true anorogenic settings (Eby, 1992). However, the high zircon inheritance detected in the Bom Sucesso and Rio do Amparo granites may indicate an extensional setting. Because as proposed by Bea et al. (2007), a high inheritance is favored by the rapid heat transfer after the intrusion of hot mantle magmas into the continental crust that can prevent zircon dissolution.

An extensional setting for the CBMC between 2750 and 2660 Ma has also been proposed by Teixeira et al. (1998) based on the existence of undeformed rocks of the Ribeirão dos Motas mafic-ultramafic unit and the gabbroic to noritic dikes in the Lavras region. In such a scenario the heat needed for melting of the crust to produce the Campo Belo granitoids could have been produced by heat advection resulting from emplacement and crystallization of basaltic magmas or by heat flux associated with mantle upwelling but also by the high contents of heat-producing elements (HPE: K, Th and U) available in these granitoids (Bea, 2012).

The southern São Francisco Craton (SSFC) may have evolved around an older crustal nucleus (ca. 3.2 Ga; Lana et al., 2013) through juvenile TTG magmatism and tectonic accretion of greenstone belt terranes that ended with the consolidation of the granitic crust between 2760 and 2680 Ma (Farina et al., 2015a, 2015b; Romano et al., 2013). According to Farina et al. (2015b), the collision of two continental blocks took place during the Mamona event (2760–2680 Ma) and accordingly, the late-Archean high-K granitoids and mantle-derived dikes in the Quadrilátero Ferrífero formed in a syn-to late-collisional geodynamic environment. In the Campo Belo metamorphic complex, located to the southwest of the Quadrilátero Ferrífero, however, the final cratonization stage is marked by the generation of high-K A-type granitoids in an extensional setting, similarly to that proposed for the generation of significant alkaline to sub-alkaline A-type magmatism in the northern sector of the São Francisco Craton (e.g., Cruz et al., 2012; Marinho et al., 2008; Santos-Pinto et al., 2012), which in turn is roughly coeval to the Campo Belo A-type granitoids.

Recently, Albert et al. (2016) have proposed a Neoproterozoic evolution model of the SSFC using O and Hf zircon isotopes combined with geochemical evidences (taken from Farina et al., 2015a) in which a change in geodynamics (transition from island arc to continental arc) took place at ~2.9 Ga, indicated by the decrease of the juvenile input to the magmatism. From that time to ~2.75 Ga a period of continental collision occurred through the accretion of various proto-continents (terrane), resulting in crustal thickening and generation of medium-K magmas via crustal reworking and differentiation. Finally, these authors proposed a change of tectonic setting at 2.75 Ga toward an extensional or non-compressional environment characterized by important crustal reworking and widespread high-K granitoid magmatism that belongs to the Mamona event (Farina et al., 2015a).

Consequently, the ages and nature of the Campo Belo granitoids reported here fit well with the crustal evolution model of the SSFC proposed by Albert et al. (2016). In the same way, comparing recent data from northern and southern São Francisco Craton reveals a similar tectono-magmatic evolution, generating extension-related A-type magmatism at similar age (2.73–2.65 Ga), for the whole craton (e.g., Cruz et al., 2012; Marinho et al., 2008; Santos-Pinto et al., 2012). However, in the Congo Craton only I-type granites were formed in post-tectonic to intracontinental settings (Shang et al., 2007; Tchameni et al., 2000).

A-type-like granitoids, although volumetrically minor, have been recognized in most Archean terranes around the world (e.g., Barros et al., 2001; Blichert-Toft et al., 1995; Champion and Sheraton, 1997; Guo et al., 2015; Mitrofanov et al., 2000; Moore et al., 1993; Shang et al., 2010; Smithies and Champion, 1999; Sutcliffe et al., 1990; Zhou et al., 2015). Despite the diachronism between cratons the alkaline igneous suites are mainly Neoproterozoic with ages younger than 2.8 Ga (c.f., Bonin, 2007). In some cases, this Neoproterozoic alkaline magmatism has been related to subduction or collision, as in the case of the 2.73–2.68 Ga amphibole-bearing granitoids from the Superior Province (Sutcliffe et al., 1990) and the ~2.75 Ga A-type granites from the Carajás Province (Barros et al., 2001; Sardinha et al., 2006). Nevertheless, this magmatism has been mainly ascribed to post-collisional and extensional settings in many other Archean terranes, such as the Yilgarn Craton (Champion and Sheraton, 1997; Smithies and Champion, 1999), the Yangtze Craton (Chen et al., 2013; Guo et al., 2015; Wang et al., 2013; Zhou et al., 2015), the Fennoscandian Shield (Heilimo et al., 2016; Mitrofanov et al., 2000; Zozulya et al., 2005), the Skjoldungen Alkaline Igneous Province (Blichert-Toft et al., 1995), the Singhbhum-Orissa Craton (Bandyopadhyay et al., 2001) and the São Francisco Craton as highlighted in this work.

7. Conclusions

The Campo Belo metamorphic complex is mainly composed of TTG migmatitic gneisses that exhibit a protracted geologic history from 3200 Ma to 3100 Ma (juvenile accretion) followed by migmatization at ca. 2840 Ma (Teixeira et al., 1998 and references therein) intruded by high-K granitoids. U-Pb ages of the main granitic plutons indicate a long period (ca. 100 My) of late Archean high-K granitoid magmatism in the complex. This started with the intrusion of a highly porphyritic biotite granitoid at ca. 2748 Ma followed by the emplacement of a hornblende-biotite granitoid at ~2727 Ma that now appear as orthogneisses. Both were affected by a deformation event prior to the emplacement of the Rio do Amparo, Bom Sucesso and Lavras granitoid plutons at ~2716 Ma, ~2696 Ma and ~2646 Ma, respectively. The Neoproterozoic granitic activity seems to end with the intrusion of leucogranitic dikes of peraluminous character at ~2631 Ma.

The Rio do Amparo, Bom Sucesso and Lavras granitoid plutons as well as the hornblende-biotite orthogneiss present A₂-type affinity and may have been formed in an extensional setting by partial melting of TTG-like sources. The characteristic high Th abundances of the Bom Sucesso and Rio do Amparo granites may imply involvement of Th-orthosilicate with minor monazite substitution in the source of these rocks. High-K granitoid magmatism also occurred at 2.73–2.65 Ga in the northern segment of the São Francisco Craton showing A₂-type affinity with distinctive enrichment in Y and Nb along with high Ce/Pb values, and in the Congo Craton with, however, I-type affinity.

Important recycling of Mesoproterozoic crust occurred during the genesis of the Campo Belo granitoids, but with probable involvement of a juvenile source. This contrasts with the Neoproterozoic

high-K magmatism from northern segment of the São Francisco Craton and from the Congo Craton characterized by negligible juvenile signature.

Stabilization of the Archean lithosphere through a major episode of high-K granitoid magmatism between 2760 and 2600 Ma marks the end of the Archean in the São Francisco Craton and the northern Congo Craton.

Acknowledgements

This work has been conducted as part of a post-doctoral grant to JAM (2014/04920-0) funded by the Fundação de Amparo à Pesquisa do Estado de São Paulo (FAPESP), Brazil. This research was funded by FAPESP thematic project “Evolution of Archean Terranes of the São Francisco Craton and the Borborema Province, Brazil: global environmental and geodynamic implications” (grant # 2012/15824-6 to EPO). JS and SKV also thank FAPESP for their grants (2014/03334-0 and 2012/07243-3, respectively). JAM would like to acknowledge José Francisco Molina for his comments and discussion on an earlier version of this manuscript. We thank Federico Farina and an anonymous reviewer for the thorough revision of the manuscript and for their insightful comments. We are also grateful to Prof. Guochun Zhao for his efficient and helpful editorial handling.

Appendix A. Supplementary data

Supplementary data associated with this article can be found, in the online version, at <http://dx.doi.org/10.1016/j.precamres.2017.04.011>.

References

- Albert, C., Farina, F., Lana, C., Stevens, G., Storey, C., Gerdes, A., Martinez Dopico, C., 2016. Archean crustal evolution in the Southern São Francisco craton, Brazil: constraints from U-Pb, Lu-Hf and O isotope analyses. *Lithos* 266–267, 64–86.
- Aguilar, C., Alkmim, F.F., Lana, C., Farina, F., 2017. Palaeoproterozoic assembly of the São Francisco craton, SE Brazil: new insights from U-Pb titanite and monazite dating. *Precamb. Res.* 289, 95–115.
- Bandyopadhyay, P.K., Chakrabarti, A.K., DeoMurari, M.P., Misra, S., 2001. 2.8 Ga old anorogenic granite-acid volcanics association from western margin of the Singhbhum-Orissa Craton, Eastern India. *Gondwana Res.* 1, 465–475.
- Barbosa, J.S.F., Sabaté, P., 2004. Archean and Paleoproterozoic crust of the São Francisco Craton, Bahia, Brazil: geodynamic features. *Precamb. Res.* 133, 1–27.
- Barros, C.E.M., Barbey, P., Boullier, A.M., 2001. Role of magma pressure, tectonic stress and crystallization progress in the emplacement of the syntectonic A-type Estrela Granite Complex (Carajás Mineral Province, Brazil). *Tectonophysics* 343, 93–109.
- Bea, F., 1996a. Controls on the trace element composition of crustal melts. *Trans. R. Soc. Edinb. Earth Sci.* 87, 33–42.
- Bea, F., 1996b. Residence of REE, Y, Th and U in granites and crustal protoliths: implications for the chemistry of crustal melts. *J. Petrol.* 37, 521–552.
- Bea, F., 2012. The sources of energy for crustal melting and the geochemistry of heat producing elements. *Lithos* 153, 278–291.
- Bea, F., Montero, P., 1999. Behavior of accessory phases and redistribution of Zr, REE, Y, Th, and U during metamorphism and partial melting of metapelites in the lower crust: an example from the Kinzigite Formation of Ivrea-Verbano, NW Italy. *Geochim. Cosmochim. Acta* 63, 1133–1153.
- Bea, F., Fershtater, G., Corretge, L.G., 1992. The geochemistry of phosphorus in granite rocks and the effect of aluminium. *Lithos* 29, 43–56.
- Bea, F., Arzamastsev, A., Montero, P., Arzamastseva, L., 2001. Anomalous alkaline rocks of Soustov, Kola: evidence of mantle-derived metasomatic fluids affecting crustal materials. *Contrib. Miner. Petrol.* 140, 554–566.
- Bea, F., Montero, P., Gonzalez Lodeiro, F., Talavera, C., 2007. Zircon inheritance reveals exceptionally fast crustal magma generation processes in Central Iberia during the Cambro-Ordovician. *J. Petrol.* 48, 2327–2339.
- Blichert-Toft, J., Rosing, M.T., Leshner, C.E., Chauvel, C., 1995. Geochemical constraints on the origin of the late Archean Skjoldungen alkaline igneous province, SE Greenland. *J. Petrol.* 36, 515–561.
- Bonin, B., 2007. A-type granites and related rocks: evolution of a concept, problems and prospects. *Lithos* 97, 1–29.
- Campos, J.C.S., 2004. O Lineamento Jeceaba-Bom Sucesso como Limite dos Terrenos Arqueanos e Paleoproterozoicos do Cráton São Francisco Meridional: Evidências Geológicas, Geoquímicas (Rocha Total) e Geocronológicas (U-Pb). Tese de Doutorado, Departamento de Geologia da Escola de Minas, Universidade Federal de Ouro Preto, p. 191.

- Campos, J.C.S., Carneiro, M.A., 2008. Neoproterozoic and Paleoproterozoic granitoids marginal to the Jeceaba-Bom Sucesso lineament (SE border of the southern São Francisco craton): genesis and tectonic evolution. *J. S. Am. Earth Sci.* 26 (4), 463–484.
- Campos, J.C.S., Carneiro, M.A., Basei, M.A.S., 2003. U-Pb evidence for Neoproterozoic crustal reworking in southern São Francisco Craton (Minas Gerais, Brazil). *Anais da Academia Brasileira de Ciências* 75, 497–511.
- Carneiro, M.A., 1992. Complexo Metamórfico Bonfim Setentrional (Quadrilátero Ferrífero, Minas Gerais): Litoestratigrafia e evolução geológica de um segmento de crosta continental do Arqueano (unpublished Ph.D. thesis). University of São Paulo, Brazil, p. 233.
- Carneiro, M.A., Teixeira, W., Carvalho Jr, I.M., Oliveira, A.H., Fernandes, R.A., 1997. Archean Sm/Nd Isochron Age from the Ribeirão dos Motas Layered Rocks Sequence, Southern São Francisco Craton, Brazil. In: *South-American Symposium on Isotope Geology. Campos do Jordão, Brazil, Extended Abstracts Volume*, pp. 63–64.
- Carneiro, M., Nalini Jr, H.A., Saita, M.T.F., Castro, P.T.A., Barbosa, M.S.C., Campos, J.C.S., Goulart, L.E.A., Silva, E.F., Perreira, A.A., Tavares, T.D., Jiamelaro, F., Carneiro, J.M., Mariano, L.C., Miguel, F.P., da Silva Jr., A.C., Barbosa, A.S., Prado, G.E.A., dos Santos, C., Urbano, E.E.M.C., 2007. Folhas Campo Belo (SF-23-V-B-VI) e Oliveira (SF-23-X-A-IV), escala 1:100.000: relatório final. Ouro Preto, 2007. Programa Geologia do Brasil: Levantamentos Geológicos Básicos.
- Carvalho, B.B., Sawyer, E.W., Janasi, V.A., 2016. Crustal reworking in a shear zone: transformation of metagranite to migmatite. *J. Metamorph. Geol.* 34, 237–264.
- Carvalho, B.B., Janasi, V.A., Sawyer, E.W., 2017. Evidence for Paleoproterozoic anatexis and crustal reworking of Archean crust in the São Francisco Craton, Brazil: a dating and isotopic study of the Kinawa migmatite. *Precamb. Res.* 291, 98–118.
- Castro, A., 2014. The off-crust origin of granite batholiths. *Geosci. Front.* 5, 63–75.
- Cederberg, J., Söderlund, U., Oliveira, E.P., Ernst, R.E., Pisarevsky, S.A., 2016. U-Pb baddeleyite dating of the Proterozoic Pará de Minas dykes in the São Francisco craton (Brazil) – implications for tectonic correlation with Siberia, Congo and the North China cratons. *GFF* 138, 219–240.
- Champion, D.C., Sheraton, J.W., 1997. Geochemistry and Nd isotope systematics of Archean of the Eastern Goldfields, Yilgarn Craton, Australia: implications for crustal growth processes. *Precamb. Res.* 83, 109–132.
- Chen, K., Gao, S., Wu, Y.B., Guo, J.L., Hu, Z.C., Liu, Y.S., Zong, K.Q., Liang, Z.W., Geng, X.L., 2013. 2.6–2.7 Ga crustal growth in Yangtze craton South China. *Precamb. Res.* 224, 472–490.
- Condie, K.C., 1993. Chemical composition and evolution of the upper continental crust: contrasting results from surface samples and shales. *Chem. Geol.* 104, 1–37.
- Cordani, U.G., 2003. From Rodinia to Gondwana: a review of the available evidence from South America. *Gondwana Res.* 6, 275–283.
- Cordani, U.G., Teixeira, W., Trindade, R.L., 2009. The position of the Amazonian Craton in supercontinents. *Gondwana Res.* 15, 396–407.
- Cotta, A., Enzweiler, J., 2009. Quantification of major and trace elements in water samples by ICP-MS and collision cell to attenuate Ar and Cl-based polyatomic ions. *J. Anal. At. Spectrom.* 24, 1406–1413.
- Cruz, S.C.P., Peucat, J.-J., Teixeira, L., Carneiro, M.A., Martins, A.A.M., Santana, J.S., Souza, J.S., Barbosa, J.S.F., Leal, A.B.M., Dantas, E., Pimentel, M., 2012. The Caraguatã syenitic suite, a ca. 2.7 Ga-old alkaline agmatism (petrology, geochemistry and U-Pb zircon ages). Southern Gavião block (São Francisco craton). *Braz. J. S. Am. Earth Sci.* 37, 1–18.
- Day, W.C., Weiblen, P.W., 1986. Origin of Late Archean granite: geochemical evidence from the Vermilion granitic complex of Northern Minnesota. *Contrib. Mineral. Petrol.* 93, 283–296.
- DePaolo, D.J., 1981. Neodymium isotopes in the Colorado Front Range and implications for crust formation and mantle evolution in the Proterozoic. *Nature* 291, 193–197.
- De Waele, B., Johnson, S.P., Pisarevsky, S.A., 2008. Palaeoproterozoic to neoproterozoic growth and evolution of the eastern Congo Craton: its role in the Rodinia puzzle. *Precamb. Res.* 160, 127–141.
- Dickinson, W., Gehrels, G., 2003. U-Pb ages of detrital zircons from Permian and Jurassic eolian sandstones of the Colorado Plateau, USA: Paleogeographic implications. *Sed. Geol.* 163, 29–66.
- Drüppel, K., McCready, A.J., Stumpf, E.F., 2009. High-K granites of the Rum Jungle Complex N-Australia: insights into the Late Archean crustal evolution of the North Australian craton. *Lithos* 111, 203–219.
- Eby, G.N., 1990. The A-type granitoids: a review of their occurrence and chemical characteristics and speculations on their petrogenesis. *Lithos* 26, 115–134.
- Eby, G.N., 1992. Chemical subdivision of A-type granitoids: petrogenetic and tectonic implications. *Geology* 20, 641–644.
- Eggs, S.M., Woodhead, J.D., Kinsley, L.P.J., Mortimer, G.E., Sylvester, P., McCulloch, M.T., Hergt, J.M., Handler, M.R., 1997. A simple method for the precise determination of >40 trace elements in geological samples by ICPMS using enriched isotope internal standardisation. *Chem. Geol.* 134, 311–326.
- Engler, A., Koller, F., Meisel, T., Quémeur, J., 2002. Evolution of the archaean/proterozoic crust in the southern São Francisco craton near Perdões, Minas Gerais, Brazil: petrological and geochemical constraints. *J. S. Am. Earth Sci.* 15, 709–723.
- Farina, F., Albert, C., Lana, C., 2015a. The Neoproterozoic transition between medium and high-K granitoids: clues from the Southern São Francisco Craton (Brazil). *Precamb. Res.* 266, 375–394.
- Farina, F., Albert, C., Martínez Dopico, C., Aguiar Gil, C., Moreira, H., Hippertt, J.P., Cutts, K., Alkmim, F.F., Lana, C., 2015b. The Archean-Paleoproterozoic evolution of the Quadrilátero Ferrífero (Brasil): current models and open questions. *J. S. Am. Earth Sci.* <http://dx.doi.org/10.1016/j.jsames.2015.10.015>.
- Frost, B.R., Frost, C.D., 2008. A geochemical classification for feldspathic igneous rocks. *J. Petrol.* 49, 1955–1969.
- Frost, C.D., Frost, B.R., 2011. On ferroan (A-type) granitoids: their compositional variability and modes of origin. *J. Petrol.* 52, 39–53.
- Frost, C.D., Frost, B.R., Chamberlain, K.R., Hulsebosch, T.P., 1998. The Late Archean history of the Wyoming province as recorded by granitic magmatism in the Wind River Range, Wyoming. *Precamb. Res.* 98, 145–173.
- Frost, B.R., Barnes, C.G., Collins, W.J., Arculus, R.J., Ellis, D.J., Frost, C.D., 2001. A geochemical classification for granitic rocks. *J. Petrol.* 42, 2033–2048.
- Goldstein, S.L., O'Nions, R.K., Hamilton, P.J., 1984. A Sm–Nd isotopic study of atmospheric dust and particulates from major river systems. *Earth Planet. Sci. Lett.* 70, 221–236.
- Goulart, L.E.A., Carneiro, M.A., Endo, I., Saita, M.T.F., 2013. New evidence of Neoproterozoic crustal growth in southern São Francisco Craton: the Carmópolis de Minas Layered Suite, Minas Gerais, Brazil. *Braz. J. Geol.* 43, 445–459.
- Govindaraju, K., Potts, P.J., Webb, P.C., Watson, J.S., 1994. 1994 Report on Whin Sill Dolerite WS-E from England and Pitscurrie Microgabbro PM-S from Scotland: assessment by one hundred and four international laboratories. *Geostand. Newslett.* 18, 211–300.
- Green, T.H., 1995. Significance of Nb/Ta as an indicator of geochemical processes in the crust–mantle system. *Chem. Geol.* 120, 347–359.
- Guo, J.L., Wu, Y.B., Gao, S., Jin, Z.M., Zong, K.Q., Hu, Z.C., Chen, K., Chen, H.H., Liu, Y.S., 2015. Epibasic Paleoproterozoic (3.3–2.0 Ga) granitoid magmatism in Yangtze Craton, South China: implications for late Archean tectonics. *Precamb. Res.* 270, 246–266.
- Harrison, T.M., Watson, E.B., 1984. The behavior of apatite during crustal anatexis: equilibrium and kinetic considerations. *Geochim. Cosmochim. Acta* 48, 1467–1478.
- Hawkesworth, C., Dhuime, B., Pietranik, A., Cawood, P., Kemp, T., Storey, C., 2010. The generation and evolution of the continental crust. *J. Geol. Soc. London* 167, 229–248.
- Hawkesworth, C., Cawood, P., Dhuime, B., 2013. Continental growth and the crustal record. *Tectonophysics* 609, 651–660.
- Heilimo, E., Mikkola, P., Huhma, H., Halla, J., 2016. Alkaline-rich quartz syenite intrusions of the Western Karelia subprovince. *Geol. Soc. Lond. Spec. Publ.* 449. <http://dx.doi.org/10.1144/SP449.4>.
- Hoffmann, J.E., Münker, C., Naeraa, T., Rosing, M.T., Herwartz, D., Garbe-Schöenberg, D., Svahnberg, H., 2011. Mechanisms of Archean crust formation inferred from high-precision HFSE systematics in TTGs. *Geochim. Cosmochim. Acta* 75, 4157–4178.
- Jayananda, M., Moyen, J.-F., Martin, H., Peucat, J.-J., Auvray, B., Mahabaleswar, B., 2000. Late Archean (2550–2520 Ma) juvenile magmatism in the Eastern Dharwar craton, southern India: constraints from geochronology, Nd–Sr isotopes and whole rock geochemistry. *Precamb. Res.* 99, 225–254.
- Jayananda, M., Chardon, D., Peucat, J.-J., Capdevila, R., 2006. 2.61 Ga potassic granites and crustal reworking in the western Dharwar craton, southern India: tectonic, geochronologic and geochemical constraints. *Precamb. Res.* 150, 1–26.
- Kemp, A.I.S., Hawkesworth, C.J., 2003. Granitic perspective on the generation and secular evolution of continental crust. *Treatise Geochem.* 3, 349–410.
- Keppler, H., Wyllie, P.J., 1991. Partitioning of Cu, Sn, Mo, W, U, and Th between melt and aqueous fluid in the systems haplogranite–H₂O–HCl and haplogranite–H₂O–HF. *Contrib. Mineral. Petrol.* 109, 139–150.
- Keppler, H., 1993. Influence of fluorine on the enrichment of high field strength trace elements in granitic rocks. *Contrib. Mineral. Petrol.* 114, 479–488.
- Kusky, T.M., Polat, A., 1999. Growth of granite–greenstone terranes at convergent margins, and stabilization of Archean cratons. *Tectonophysics* 305, 43–73.
- Lana, C., Alkmim, F.F., Armstrong, R., Scholz, R., Romano, R., Nalini, H.A., 2013. The ancestry and magmatic evolution of Archean TTG rocks of the Quadrilátero Ferrífero province, southeast Brazil. *Precamb. Res.* 231, 157–173.
- Laurent, O., Martin, H., Moyen, J.F., Doucelance, R., 2014a. The diversity and evolution of late-Archean granitoids: evidence for the onset of “modern-style” plate tectonic between 3.0 and 2.5 Ga. *Lithos* 205, 208–235.
- Laurent, O., Rapoport, M., Stevens, G., Moyen, J.F., Martin, H., Doucelance, R., Bosq, C., 2014b. Contrasting petrogenesis of Mg–K and Fe–K granitoids and implications for postcollisional magmatism: a case study from the late-Archean Matok pluton (Pietersburg block, South Africa). *Lithos* 196–197, 131–149.
- Liang, Q., Jing, H., Gregoire, D.C., 2000. Determination of trace elements in granites by inductively coupled plasma mass spectrometry. *Talanta* 51, 507–513.
- Lopes, G.A.C., 2002. Projeto Guajeru, 1. CBPM, Salvador, p. 408p.
- Machado, N., Carneiro, M.A., 1992. U-Pb evidence of Late Archean tectonothermal activity in southern São Francisco shield, Brazil. *Can. J. Earth Sci.* 29, 2341–2346.
- Machado, N., Noce, C.M., Ladeira, E.A., Belo de Oliveira, O.A., 1992. U-Pb geochronology of Archean magmatism and Proterozoic metamorphism in the Quadrilátero Ferrífero, Southern São Francisco craton, Brazil. *Geol. Soc. Am. Bull.* 104, 1221–1227.
- Machado, N., Schrank, A., Noce, C.M., Gauthier, G., 1996. Ages of detrital zircon from Archean-Paleoproterozoic sequences: implications for greenstone belt setting and evolution of a Transamazonian foreland basin in Quadrilátero Ferrífero, southeast Brazil. *Earth Planet. Sci. Lett.* 141, 259–276.
- Marinho, M.M., Rios, D.C., Conceição, H., Rosa, M.L.S., 2008. Magmatismo alcalino neoproterozoico no Cráton do São Francisco, Bahia: pluton Pé de Serra. *SBG, Congresso Brasileiro de Geologia*, vol. 44. Anais, p. 57.

- Martin, R.F., 2006. A-type granites of crustal origin ultimately result from open-system fenitization-type reactions in an extensional environment. *Lithos* 91, 125–136.
- McDonough, W.F., Sun, S.S., 1995. The composition of the Earth. *Chem. Geol.* 120, 223–253.
- Mikkola, P., Huhma, H., Heilimo, E., Whitehouse, M., 2011. Archean crustal evolution of the Suomussalmi district as part of the Kianta Complex, Karelia: constraints from geochemistry and isotopes of granitoids. *Lithos* 125, 287–307.
- Mitrofanov, F.P., Zozulya, D.R., Bayanova, T.B., Levkovich, N.V., 2000. The world's oldest anorogenic alkali granitic magmatism in the keivy structure on the Baltic shield. *Geochemistry* 374, 238–241.
- Montero, P., Bea, F., 1998. Accurate determination of $^{87}\text{Rb}/^{86}\text{Sr}$ and $^{147}\text{Sm}/^{144}\text{Nd}$ ratios by inductively-coupled-plasma mass spectrometry in isotope geoscience: an alternative to isotope dilution analysis. *Anal. Chim. Acta* 358, 227–233.
- Montero, P., Bea, F., Corrette, L.G., Floor, P., Whitehouse, M.J., 2009. U-Pb ion microprobe dating and Sr–Nd isotope geology of the Galileio Igneous Complex. A model for the peraluminous/peralkaline duality of the Cambro-Ordovician magmatism of Iberia. *Lithos* 107, 227–238.
- Moore, M., Davis, D.W., Robb, L.J., Jackson, M.C., Grobler, D.F., 1993. Archean rapakivi granite–anorthosite–rhyolite complex in the Witwatersrand basin hinterland, southern Africa. *Geology* 21, 1031–1034.
- Moreira, H., Lana, C., Nalini Jr., H.A., 2016. The detrital zircon record of an Archean convergent basin in the Southern São Francisco Craton Brazil. *Precamb. Res.* 275, 84–99.
- Moreno, J.A., Montero, P., Abu Anbar, M., Molina, J.F., Scarrow, J.H., Talavera, C., Cambeses, A., Bea, F., 2012. SHRIMP U-Pb zircon dating of the Katerina Ring Complex: insights into the temporal sequence of Ediacaran calc-alkaline to peralkaline magmatism in southern Sinai, Egypt. *Gondwana Res.* 21, 887–900.
- Moreno, J.A., Molina, J.F., Montero, P., Abu Anbar, M., Scarrow, J.H., Cambeses, A., Bea, F., 2014. Unraveling sources of A-type magmas in juvenile continental crust: constraints from compositionally diverse Ediacaran post-collisional granitoids in the Katerina Ring Complex, southern Sinai, Egypt. *Lithos* 192–195, 56–85.
- Moreno, J.A., Molina, J.F., Bea, F., Anbar, M., Abu, Montero, P., 2016. Th–REE- and Nb–Ta-accessory minerals in post-collisional Ediacaran felsic rocks from the Katerina Ring Complex (S. Sinai, Egypt): an assessment for the fractionation of Y/Nb, Th/Nb, La/Nb and Ce/Pb in highly evolved A-type granites. *Lithos* 258–259, 173–196.
- Moyen, J.-F., Martin, H., Jayananda, M., Auvray, B., 2003. Late Archean granites: a typology based on the Dharwar Craton (India). *Precamb. Res.* 127, 103–123.
- Noce, C.M., 1995. Geocronologia dos eventos magmáticos, sedimentares e metamórficos na região do Quadrilátero Ferrífero, Minas Gerais (unpublished Ph.D. theses). University of São Paulo, Minas Gerais, Brazil, p. 129.
- Noce, C.M., Machado, N., Teixeira, W., 1998. U-Pb geochronology of gneisses and granitoids in the Quadrilátero Ferrífero (Southern São Francisco Craton): age constraints for Archean and Paleoproterozoic magmatism and metamorphism. *Rev. Bras. Geoci.* 28, 95–102.
- Noce, C.M., Teixeira, W., Quéméneur, J.J., Martins, V.T., Bolzachini, É., 2000. Isotopic signatures of Paleoproterozoic granitoids from the southern São Francisco Craton and implications for the evolution of the Transamazonian Orogeny. *J. S. Am. Earth Sci.* 13, 225–239.
- Oliveira, A.H., Carneiro, M.A., 2001. Campo Belo Metamorphic Complex: Evolution of an Archean sialic crust of the southern São Francisco Craton in Minas Gerais (Brazil). *Anais da Academia Brasileira de Ciências* 73 (3), 397–415.
- Paton, C., Woodhead, J.D., Hellstrom, J.C., Hergt, J.M., Greig, A., Maas, R., 2010. Improved laser ablation U-Pb zircon geochronology through robust downhole fractionation correction. *Geochim. Geophys. Geosyst.* 11, 1–36.
- Petrus, J.A., Kamber, B.S., 2012. VizualAge: a novel approach to laser ablation ICP-MS U-Pb geochronology data reduction. *Geostand. Geoanal. Res.* 36, 247–270.
- Pinese, J.P.P., 1997. Geoquímica, Geologia Isotópica e aspectos petrológicos dos diques máficos pré-Cambrianos da região de Lavras (MG), porção sul do Craton do São Francisco (unpublished Ph.D. thesis). Institute of Geosciences, University of São Paulo, São Paulo, Brazil, p. 178.
- Pinese, J.P.P., Teixeira, W., Piccirillo, E.M., Quéméneur, J.J.G., Bellieni, G., 1995. The Precambrian Lavras mafic dykes, southern São Francisco Craton, Brazil: preliminary geochemical and geochronological results. In: Baer, G., Heimann, A. (Eds.), *Physics and Chemistry of Dykes*, pp. 205–218. Rotterdam – Netherlands.
- Quéméneur, J.J.G., 1996. Os magmatismos de idade arqueana e transamazônica na região Campos das Vertentes, MG (sul do Cráton São Francisco), com base em geoquímica e geocronologia. Tese de Livre Docência, Instituto de Geociências, Universidade Federal de Minas Gerais, p. 79.
- Romano, R., Lana, C., Alkmim, F.F., Stevens, G.S., Armstrong, R., 2013. Stabilization of the southern portion of the São Francisco Craton, SE Brazil, through a long-lived period of potassic magmatism. *Precamb. Res.* 224, 143–159.
- Santos-Pinto, M., Peucat, J.J., Martin, H., Barbosa, J.S.F., Fanning, C.M., Cocherie, A., Paquette, J.L., 2012. Crustal evolution between 2.0 and 3.5 Ga in the southern Gavião block (Umburanas-Brumado-Aracatu region), São Francisco Craton, Brazil. A 3.5–3.8 Ga proto-crust in the Gavião block? *J. S. Am. Earth Sci.* 40, 129–142.
- Sardinha, A.S., Barros, C.E.M., Krymsky, R., 2006. Geology, geochemistry, and U-Pb geochronology of the archaic (2.74 Ga) Serra do Rabo granite stocks, Carajás Province, northern Brazil. *J. S. Am. Earth Sci.* 20, 327–339.
- Semprich, J., Moreno, J.A., Oliveira, E.P., 2015. Phase equilibria and trace element modeling of Archean sanukitoid melts. *Precamb. Res.* 269, 122–138.
- Shang, C.K., Liégeois, J.P., Satir, M., Frisch, W., Nsifa, E.N., 2010. Late Archean high-K granite geochronology of the northern metacratonic margin of the Archean Congo craton, southern Cameroon: evidence for Pb-loss due to non-metamorphic causes. *Gondwana Res.* 18, 337–355.
- Shang, C.K., Satir, M., Nsifa, E.N., Liégeois, J.P., Siebel, W., Taubald, H., 2007. Archean high-K granitoids produced by remelting of the earlier Tonalite–Trondhjemite–Granodiorite (TTG) in the Sangmelima region of the Ntem complex of the Congo craton, southern Cameroon. *Int. J. Earth Sci.* 96, 817–842.
- Smithies, R.H., Champion, D.C., 1999. Late Archean felsic alkaline igneous rocks in the Eastern Goldfields, Yilgarn Craton, Western Australia: a result of lower crustal delamination? *J. Geol. Soc.* 156, 561–576.
- Smithies, R.H., Champion, D.C., 2000. The Archean high-Mg diorite suite: links to tonalite–trondhjemite–granodiorite magmatism and implications for early Archean crustal growth. *J. Petrol.* 41 (12), 1653–1671.
- Stepanov, A.S., Hermann, J., Rubatto, D., Rapp, R.P., 2012. Experimental study of monazite/melt partitioning with implications for the REE, Th and U geochemistry of crustal rocks. *Chem. Geol.* 300–301, 200–220.
- Stern, R.A., Hanson, G.N., Shirey, S.B., 1989. Petrogenesis of mantle-derived, LILE enriched Archean monzodiorites and trachyandesites (sanukitoids) in southwestern Superior Province, Can. *J. Earth Sci.* 26, 1688–1712.
- Stern, R.J., 2002. Crustal evolution in the East African Orogen: a neodymium isotopic perspective. *J. Afr. Earth Sc.* 34, 109–117.
- Sutcliffe, R.H., Smith, A.R., Doherty, W., Barnett, R.L., 1990. Mantle derivation of Archean amphibole-bearing granitoid and associated mafic rocks: evidence from the southern Superior Province, Canada. *Contrib. Miner. Petrol.* 105, 255–274.
- Sylvester, P.J., 1989. Post-collisional alkaline granites. *J. Geol.* 97, 261–280.
- Sylvester, P.J., 1994. Archean granite plutons. In: Condie, K.C. (Ed.), *Archean Crustal Evolution. Developments in Precambrian Geology*, vol. 11. Elsevier, Amsterdam, pp. 261–314.
- Tchameni, R., Mezger, K., Nsifa, N.E., Poulet, A., 2000. Neoproterozoic evolution in the Congo craton: evidence from K rich granitoids of the Ntem complex, Southern Cameroon. *J. Afr. Earth Sc.* 30, 133–147.
- Teixeira, W., Figueiredo, M.C.H., 1991. An outline of Early Proterozoic crustal evolution in the São Francisco Craton, Brazil: a review. *Precamb. Res.* 53, 1–22.
- Teixeira, W., Carneiro, M.A., Noce, C.M., Machado, N., Sato, K., Taylor, P.N., 1996. Pb, Sr and Nd isotope constraints on the Archean evolution of gneissic-granitoid complexes in the southern São Francisco Craton, Brazil. *Precamb. Res.* 78, 151–164.
- Teixeira, W., Cordani, U.G., Nutman, A.P., Sato, K., 1998. Polyphase Archean evolution in the Campo Belo Metamorphic Complex, Southern São Francisco Craton, Brazil: SHRIMP U-Pb zircon evidence. *J. S. Am. Earth Sci.* 11, 279–289.
- Teixeira, W., Sabatê, P., Barbosa, J., Noce, C.M., Carneiro, M.A., 2000. Archean and Paleoproterozoic evolution of the São Francisco Craton, Brazil. In: U.G. Cordani, E.J. Milani, A. Thomaz Filho, D.A. Campos (Eds.), *Tectonic Evolution of South America. 31st International Geological Congress*, pp. 101–137.
- Teixeira, W., Oliveira, E.P., Peng, P., Dantas, E.L., Hollanda, M.H.M., 2017. U-Pb geochronology of the 2.0 Ga Itapeçerica graphitic succession in the São Francisco Craton: geologic matches with the North China Craton and global implications. *Precamb. Res.* <http://dx.doi.org/10.1016/j.precamres.2017.02.021>.
- Trouw, R.A.J., Paciullo, F.V.P., Ribeiro, A., Cherman, A., Chrispim, S., Maciel, R.R., 2008. Folha Nepomucen (SF.23-V-D-III), escala 1:100.000: relatório final. Rio de Janeiro, 2007. Programa Geologia do Brasil: Levantamentos Geológicos Básicos.
- Vendemiaatto, M.A., Enzweiler, J., 2001. Routine control of accuracy in silicate rock analysis by X-ray fluorescence spectrometry. *Geostand. Newslett.* 25, 283–291.
- Verma, S.P., Pandarinath, K., Verma, S.K., Agrawal, S., 2013. Fifteen new discriminant-function-based multi-dimensional robust diagrams for acid rocks and their application to Precambrian rocks. *Lithos* 168–169, 113–123.
- Wang, Z.J., Wang, J., Du, Q.D., Deng, Q., Yang, F., 2013. The evolution of the Central Yangtze Block during early Neoproterozoic time: evidence from geochronology and geochemistry. *J. Asian Earth Sci.* 77, 31–44.
- Watson, E.B., Harrison, T.M., 1983. Zircon saturation revisited: temperature and composition effects in a variety of crustal magma types. *Earth Planet. Sci. Lett.* 64, 295–304.
- Whalen, J.B., Currie, K.L., Chappell, B.W., 1987. A-type granites: geochemical characteristics, discrimination and petrogenesis. *Contrib. Miner. Petrol.* 95, 407–419.
- Wiedenbeck, M., Allé, P., Corfu, F., Griffin, W.L., Meier, M., Oberli, F., Von, Q.A., Roddick, J.C., Spiegel, W., 1995. Three natural zircon standards for U–Th–Pb, Lu–Hf, trace element and REE analyses. *Geostand. Newslett.* 19, 1–23.
- Zhou, G.Y., Wu, Y.B., Gao, S., Yang, J.Z., Zheng, J.P., Qin, Z.W., Wang, H., Yang, S.H., 2015. The 2.65 Ga A-type granite in the northeastern Yangtze craton: Petrogenesis and geological implications. *Precamb. Res.* 258, 247–259.
- Zozulya, D.R., Bayanova, T.B., Eby, G.N., 2005. Geology and age of the Late Archean Keivy alkaline province, Northeastern Baltic Shield. *J. Geol.* 113, 601–608.